Available online at www.sciencedirect.com
SCIENCE DIRECT®
ELSEVIER
International Journal of Solids and Structures 43 (2006) 3350–3380
INTERNATIONAL JOURNAL OF SOLIDS and STRUCTURES
www.elsevier.com/locate/ijsolstr

A rate-dependent damage model for brittle materials based on the dominant crack

Q.H. Zuo [a,*], F.L. Addessio [a], J.K. Dienes [a], M.W. Lewis [b]

[a] *Theoretical Division, Los Alamos National Laboratory, MS B216, Los Alamos, NM 87545, USA*
[b] *Engineering Sciences and Applications Division, Los Alamos National Laboratory, MS P946, Los Alamos, NM 87545, USA*

Received 20 February 2005; received in revised form 29 June 2005
Available online 30 August 2005

Abstract

A rate-dependent, continuum damage model is developed for brittle materials under dynamic loading. This model improves on the approach (ISOSCM) of [Addessio, F.L., Johnson, J.N., 1990. A constitutive model for the dynamic response of brittle materials. Journal of Applied Physics 67, 3275–3286] in several respects. (1) A new damage surface is found by applying the generalized Griffith instability criterion to the dominant crack (having the most unstable orientation), rather than by averaging the instability condition over all crack orientations as done previously. The new surface removes a discontinuity in the damage surface in ISOSCM when the pressure changes sign. (2) The strain due to crack opening is more consistent with crack mechanics, with only the tensile principal stresses contributing to the crack opening strain. This is achieved by incorporating a projection operator in the equation for the crack opening strain. One consequence of incorporating the projection operator is a prediction of shear dilatancy, which is not accounted for in ISOSCM. (3) The evolution of damage, which is based on the energy-release rate for the dominant crack, has a physical basis, whereas in the previous approach the damage growth rate was assumed to be an exponential function of the distance from the stress state to the damage surface without specific physical justification.

An implicit algorithm has been developed so that a larger time step can be used than with the explicit algorithm used in ISOSCM. The numerical results of a silicon carbide (SiC) ceramic under several loading paths (hydrostatic tension/compression, uniaxial strain, uniaxial stress, and shear) and strain rates are presented to illustrate the main features of the model.

Keywords: Damage model; Brittle materials; Crack strains; Distribution of microcracks; Penny-shaped cracks; Crack instability

* Corresponding author. Tel.: +1 505 667 0377; fax: +1 505 665 5926.
E-mail address: zuo@lanl.gov (Q.H. Zuo).

0020-7683/$ - see front matter © 2005 Elsevier Ltd. All rights reserved.
doi:10.1016/j.ijsolstr.2005.06.083

1. Introduction

Brittle or quasi-brittle materials (e.g., ceramics, high explosives, beryllium alloys, concretes, rocks, and many composites) are increasingly used as structural components for civil and defense applications. For example, in an effort to reduce weight and improve mobility, modern armor designers often rely on light-weight ceramics to provide effective protection. Ceramics are brittle materials with very high compressive strength (particularly under confinement and high loading rate), but low tensile strength. Furthermore, at high strain rates or sufficiently low temperature even materials that would normally be considered ductile exhibit brittle behavior. Understanding and predicting brittle failure are critical to prevent catastrophic engineering disasters. Consequently, modeling damage and failure of brittle or quasi-brittle materials has received considerable attention recently from the mechanics and materials community. For example, Dube et al. (1996) developed a rate-dependent damage model for concrete (a quasi-brittle material) under dynamic loading which can reproduce the major effects of the loading rate on the concrete response. Zhang et al. (2003) proposed an anisotropic model for predicting dynamic damage and fragmentation of rock materials under explosive loading. Their model provides a quantitative method to estimate the fragmentation distribution and fragment size generated by crack coalescence in the dynamic fragmentation process.

The modeling approaches range from the simplest ad hoc or empirical models to micromechanics-based approaches, which lead to more accurate, often tensorial description, of material responses. The phenomenological approach, which has been increasingly used in constructing damage models, typically starts by postulating thermodynamic potentials and uses irreversible-thermodynamics arguments to derive evolution equations for the damage variables (e.g., Simo and Ju, 1987, 1989; Lemaitre and Chaboche, 1990; Krajcinovic, 1984, 1989, 1996, 1998; Hansen and Schreyer, 1994, 1995). The micromechanical approach typically starts with the behavior of a single defect (crack or void) and the continuum level model is obtained by applying statistical averaging to an ensemble of defects (e.g., Seaman et al., 1976, 1985; Dienes, 1978, 1996; Dienes and Margolin, 1980; Costin, 1983; Grady and Kipp, 1985; Taylor et al., 1986; Rajendran and Kroupa, 1989; Rajendran, 1994; Rajendran and Grove, 1996; Addessio and Johnson, 1990; Gambarotta and Lagomarsino, 1993; Lewis and Schreyer, 1996; Bennett et al., 1998; Hackett and Bennett, 2000; Krajcinovic, 1998; Lee et al., 2004).

One example of micromechanical material models is Statistical Crack Mechanics (SCRAM), the theoretical approach developed by Dienes (1978), Dienes and Margolin (1980), Dienes (1981, 1983a, 1989, 1996) for modeling dynamic deformation and fragmentation of brittle materials. It accounts for the opening, shear, growth, and coalescence of an ensemble of cracks. The crack distribution in the material is typically assumed to be initially isotropic (though the theory allows for an initially anisotropic distribution of cracks, as in oil shale), and the anisotropy of damage is captured by tracking the evolution of mean crack sizes with several (typically 9) orientations. The SCRAM model has been used to explain the formation of an aspirin-shaped cavity in oil shale (Dienes, 1981), a result of bedding cracks, the violent explosions in solid propellants caused by mild mechanical shocks such as XDT (since the cause of the detonation transition was unknown, Dienes, 1996), and the damage and failure of a ceramic armor under ballistic impact (Meyer et al., 1999; Zuo et al., 2003).

Based on Dienes' SCRAM theory, Addessio and Johnson (1990) proposed a simplified, isotropic damage model (ISOSCM) for the dynamic response of brittle materials under nearly isotropic stress states (e.g., the state produced during high-velocity plate impact). They assumed that during the damage process the distribution of cracks remains isotropic, and that the crack probability-density function is exponential in crack size. Macroscopic crack strains and an isotropic damage surface were found by averaging the crack strains as well as the instability condition for a single crack under a remote stress field over all crack orientations. The resulting isotropic damage surface involves only the mean crack size, the von Mises stress, and pressure, and takes two different forms depending on the sign of the pressure (p). In compression ($p > 0$), for large values of the mean crack size the damage surface approaches the Drucker-Prager plastic yield surface

for granular materials. In tension ($p < 0$), the damage surface resembles the Gurson surface, which describes damage in ductile materials due to tensile void growth. The model can be viewed as a continuum damage model with the damage variable defined by the initial crack-number density, which is assumed to remain constant during deformation, and the mean crack size in the material. The evolution of material damage is given through the growth of mean crack size when the stress state is outside the damage surface. That model is compatible with the incremental continuum formulation inherent to existing design computer codes, and can be easily implemented into such codes. The model was applied to simulate damage in ceramics (silicon carbide, boron carbide, and titanium diboride) under impact conditions, and the predictions compared favorably with shock compression and release experiments (Kipp and Grady, 1989a,b; Grady, 1989). Due to its numerical efficiency, mathematical simplicity, and origin in micromechanics, the model has been adopted by other researchers as the starting point for developing their own damage models for brittle materials (e.g., Bennett et al., 1998; Hackett and Bennett, 2000; Rajendran and Grove, 1996; Lee et al., 2004). Bennett et al. extended ISOSCM to include the viscous effects of the binder materials in a plastic bonded explosive and applied their model (Visco-SCRAM) to study non-shock ignition (formation of explosive hot spots) and mechanical response of explosives. Most recently, Lee et al. (2004) adopted the damage surface and the crack growth rate in ISOSCM as a part of their model for damage and crushing of chopped random fiber composites. They also included nucleation of microcracks and debonding between fibers and composites.

Three issues in ISOSCM have warranted further investigation presented here:

1. A discontinuity in the damage surface when the pressure in the material changes sign.
2. In crack mechanics, when the principal stresses have mixed signs, cracks with some orientations are under tension and open, while others are under compression and stay closed. Only the open cracks contribute to the crack-opening strain. In ISOSCM, however, whether or not a crack contributes to the crack-opening strain depends solely on the sign of the pressure, not on the crack orientation. That is, when the pressure is negative (tension), all crack orientations contribute even though cracks with some orientations are under compression and do not open.
3. Damage accumulates when the stress states is outside the damage surface. The damage growth rate was assumed to be an exponential function of the distance of the stress state from the surface. The formulation is appealing in that it is analogous to the over-stress model for rate-dependent plasticity and provides a length scale, which can be beneficial to the solution of problems involving strain-softening due to damage. However, physical justification for using such an over-stress model for damage growth was not provided.

As discussed by Lewis and Schreyer (1996), the first two issues can lead to thermodynamic inconsistency which is manifested as energy creation under certain cyclic load paths. The main object of the current work is to develop a new damage model, which is more physically based and removes those inconsistencies in ISOSCM. Specifically, in the current work, instead of averaging the crack instability condition over all crack orientations, the damage surface is obtained by applying the instability condition to the dominant crack. The dominant crack is defined here as the crack with the critical (most unstable) orientation which evolves with the applied stress. In recent work (Zuo and Dienes, 2002, 2005), we have determined the critical crack orientation analytically for all possible stress states, and have presented the damage surface, $F(\boldsymbol{\sigma}, \bar{c}) = 0$, in terms of the applied stress and crack size. We use an extended Griffith instability criterion (Keer, 1966; Rice, 1984), which applies to both open cracks and closed cracks with friction. The new damage surface removes the discontinuity in the previous model and has many features that characterize brittle behavior.

The crack-opening strain is now accounted for more accurately in that, when the principal stresses have mixed signs, only the tensile principal stresses contribute to the crack-opening strain. This is achieved by

using the idea of activated crack-opening strain proposed by Lewis (1991), which is based on the damage deactivation work of Hansen and Schreyer (1994, 1995) and on the numerical results of Lewis and Schreyer (1996) on crack-opening strain.

For stress states outside the damage surface ($F(\boldsymbol{\sigma}, \bar{c}) > 0$), the material accumulates additional damage. Based on the results of dynamic crack growth (Freund, 1972, 1990), the evolution of damage (growth of average crack size) is now given as a function of the energy-release rate for crack with the critical orientation. This current formulation is analogous to an over-stress model for rate-dependent plasticity.

The mathematical formulation of the model is presented in Sections 2. The numerical algorithm used to integrate the model is discussed in Section 3. An implicit algorithm has been developed for the model so that large time steps may be used in engineering analyses. Example problems are provided in Section 4. Some conclusions are drawn in Section 5.

2. Model formulation

2.1. Crack strain

Consider an ensemble of penny-shaped microcracks which are randomly distributed within a statistically homogenous volume of a brittle material under a multiaxial loading. The requirements for a material volume to be statistically homogenous are those discussed by Krajcinovic (1998). That is, the number of defects (cracks) and heterogeneities within the material volume must be large and their locations and orientations must be random (uncorrelated) and their size small compared to separation. The applied stress may cause the opposite faces of cracks to slide and/or open, resulting in an additional strain (crack strain), and an increase of material compliance. The change in the macroscopic compliance due to an ensemble of microcracks has been studied extensively in the past 30 years (e.g., Budiansky and O'Connell, 1976; Dienes, 1978, 1981, 1983a, 1989, 1996; Dienes and Margolin, 1980; Oda, 1983; Oda et al., 1984; Kachanov, 1993). Many important results from these studies can be found in the research monographs by Krajcinovic (1996) and Nemat-Nasser and Hori (1999). The increment of the mean strain (in the sense of an ensemble average) due to a homogenous distribution of similar penny-shaped cracks (i.e., a crack set) with the unit normal $\mathbf{n}$ and radius c, is (Dienes, 1989, 1996)

$$\Delta\boldsymbol{\varepsilon}_{\mathrm{c}}(\boldsymbol{\sigma}, c, \mathbf{n}, t) = \Delta\boldsymbol{\varepsilon}_{c}^{\mathrm{o}}(\boldsymbol{\sigma}, c, \mathbf{n}, t) + \Delta\boldsymbol{\varepsilon}_{\mathrm{c}}^{\mathrm{s}}(\boldsymbol{\sigma}, c, \mathbf{n}, t) = n(c, \mathbf{n}, t)\Delta c \Delta\Omega \alpha^{\mathrm{e}} c^{3} \mathbf{b}(\boldsymbol{\sigma}, \mathbf{n}), \tag{1a}$$

$$\mathbf{b}(\boldsymbol{\sigma}, \mathbf{n}) = (2 - \nu) < \mathbf{n} \cdot \boldsymbol{\sigma}\mathbf{n} > \mathbf{n} \otimes \mathbf{n} + (\boldsymbol{\sigma}\mathbf{n}) \otimes \mathbf{n} + \mathbf{n} \otimes (\sigma\mathbf{n}) - 2(\mathbf{n} \cdot \boldsymbol{\sigma}\mathbf{n})\mathbf{n} \otimes \mathbf{n}, \tag{1b}$$

where $\boldsymbol{\sigma}$ is the far-field Cauchy stress and the angled bracket is the Macaulay bracket, which takes the value of the argument when positive and is zero otherwise. In the equation, $\alpha^{e} \equiv 8(1 - \nu)/[3G(2 - \nu)]$, is a constant arising from analytic solutions for open and closed penny-shaped cracks (Sack, 1946; Segedin, 1950; Keer, 1966), and G and ν are the elastic shear modulus and Poisson's ratio of the matrix (undamaged) material, respectively. $n(c, \mathbf{n}, t)$ is the number density defining the distribution of crack radii and orientations, which evolves with the time t. That is, $n(c, \mathbf{n}, t)\Delta c \Delta\Omega$ represents the number density of cracks (number of cracks per unit volume) whose radii are between c and $c + \Delta c$, and have a unit normal within a small solid angle $\Delta\Omega$ around $\mathbf{n}$ (e.g., Oda, 1983; Dienes, 1985). In Eq. (1b), the symbol $\otimes$ denotes the tensor product so that $(\boldsymbol{\sigma}\mathbf{n}) \otimes \mathbf{n} = (\sigma_{ik} n_k n_j)\mathbf{e}_i \otimes \mathbf{e}_j$ and $\mathbf{n} \otimes (\boldsymbol{\sigma}\mathbf{n}) = (n_i \sigma_{jk} n_k)\mathbf{e}_i \otimes \mathbf{e}_j$. For the sake of compactness, the direct notation for tensors and vectors (e.g., Gurtin, 1981) is used throughout this paper.

For an open crack ($\sigma_n = \mathbf{n} \cdot (\boldsymbol{\sigma}\mathbf{n}) = n_i \sigma_{ij} n_j > 0$), a rather special case of $\nu = 0$ corresponds to a particularly simple form of Eq. (1), which was used by Oda et al. (1984) in formulating fabric tensors. Neglecting the interactions between cracks (Kachanov, 1993), the total crack strain due to an ensemble of microcracks of all sizes and orientations is obtained by summing the contributions in Eq. (1) over crack size ($0 \leqslant c \leqslant \infty$) and orientations (Dienes, 1989, 1996)

$$\boldsymbol{\varepsilon}_{\mathrm{c}}(\boldsymbol{\sigma},t)=\sum_{\Omega,c}\Delta\boldsymbol{\varepsilon}_{\mathrm{c}}(\boldsymbol{\sigma},c,\mathbf{n},t)\approx\int_{\Omega}\int_{c}\alpha^{\mathrm{e}}c^{3}\mathbf{b}(\boldsymbol{\sigma},\mathbf{n})n(c,\mathbf{n},t)\,\mathrm{d}c\,\mathrm{d}\Omega. \tag{2}$$

In terms of the usual polar coordinates (Euler angles) θ and ϕ of the normal vector $\mathbf{n}$, the incremental solid angle is the area of an element on the unit sphere, $\mathrm{d}\Omega=\sin\phi\,\mathrm{d}\theta\,\mathrm{d}\phi$. Cracks have symmetry such that a reversal of 180° leaves them unchanged. Thus, half the unit sphere is sufficient to characterize crack orientation; consequently, the integration limits for orientation are $0\leqslant\theta\leqslant2\pi$ and $0\leqslant\phi\leqslant\pi/2$. Experiments (Seaman et al., 1976; Curran et al., 1987; Curran and Seaman, 1996; Scholz, 2002) indicate that the crack number density function can often be approximated by an exponential function

$$n(c,\mathbf{n},t)=\frac{N_0(\mathbf{n})}{\bar{c}(\mathbf{n},t)}\exp(-c/\bar{c}(\mathbf{n},t)), \tag{3}$$

where $\bar{c}(\mathbf{n},t)$ is the average crack radius, and $N_0(\mathbf{n})$ is the initial crack number density per solid angle for crack orientation $\mathbf{n}$. The number of cracks per unit volume is then $\widehat{N}_0=\int_{\Omega}\int_{c}n(c,\mathbf{n},t)\,\mathrm{d}c\,\mathrm{d}\Omega=\int_{\Omega}N_0(\mathbf{n})\,\mathrm{d}\Omega$, which remains constant over time (i.e., there is no crack nucleation or coalescence during deformation). It follows from Eq. (3) that for a given orientation $\mathbf{n}$, the number density of cracks with radius larger than c is $N(c,\mathbf{n},t)=\int_{c}^{\infty}n(c,\mathbf{n},t)\,\mathrm{d}c=N_0(\mathbf{n})\exp(-c/\bar{c}(\mathbf{n},t))$, which decreases exponentially with the crack radius.

Following Addessio and Johnson (1990), it is also assumed here that the crack density distribution follows Eq. (3) and that cracks of all sizes are initially present in the material. Consequently, the damage is characterized by the average crack radius $\bar{c}(\mathbf{n},t)$, which evolves with time t. Material anisotropy is reflected in the dependency of $\bar{c}(\mathbf{n},t)$ on the crack orientation $\mathbf{n}$ (e.g., when material spall occurs in plate-impact experiments, $\bar{c}(\mathbf{n},t)$ would be concentrated in the direction of impact; at the other extreme, when the material is under hydrostatic tension and cracks become unstable, $\bar{c}(\mathbf{n},t)$ would increase with time, but is independent of the crack orientation $\mathbf{n}$).

Substituting $\mathbf{b}(\boldsymbol{\sigma},\mathbf{n})$ and $n(c,\mathbf{n},t)$ given by Eqs. (1b) and (3), respectively, into Eq. (2) and carrying out the integrations over the crack radius c gives the total crack strain as

$$\boldsymbol{\varepsilon}_{\mathrm{c}}(\boldsymbol{\sigma},t)=\boldsymbol{\varepsilon}_{\mathrm{c}}^{\mathrm{o}}(\boldsymbol{\sigma},t)+\boldsymbol{\varepsilon}_{\mathrm{c}}^{\mathrm{s}}(\boldsymbol{\sigma},t), \tag{4}$$

with the open crack strain and shear crack strain given by

$$\boldsymbol{\varepsilon}_{\mathrm{c}}^{\mathrm{o}}(\boldsymbol{\sigma},t)=\frac{16}{G}(1-\nu)\int_{\Omega}N_0(\mathbf{n})\bar{c}^{3}(\mathbf{n},t)<\mathbf{n}\cdot\boldsymbol{\sigma}\mathbf{n}>\mathbf{n}\otimes\mathbf{n}\,\mathrm{d}\Omega, \tag{5a}$$

$$\boldsymbol{\varepsilon}_{\mathrm{c}}^{\mathrm{s}}(\boldsymbol{\sigma},t)=\frac{16}{G}\frac{1-\nu}{2-\nu}\int_{\Omega}N_0(\mathbf{n})\bar{c}^{3}(\mathbf{n},t)\{(\boldsymbol{\sigma}\mathbf{n})\otimes\mathbf{n}+\mathbf{n}\otimes(\boldsymbol{\sigma}\mathbf{n})-2(\mathbf{n}\cdot\boldsymbol{\sigma}\mathbf{n})\mathbf{n}\otimes\mathbf{n}\}\,\mathrm{d}\Omega. \tag{5b}$$

$\boldsymbol{\varepsilon}_{\mathrm{c}}^{\mathrm{s}}(\boldsymbol{\sigma},t)$ is a deviatoric tensor (i.e., $\mathrm{tr}\,\boldsymbol{\varepsilon}_{\mathrm{c}}^{\mathrm{s}}(\boldsymbol{\sigma},t)=0$), i.e., the sliding of crack faces does not contribute to dilatancy; however, this does not imply that the theory precludes shear dilatancy (positive volumetric strain). Under a pure-shear state of stress, because the maximum principal stress is tensile, there is a range of crack orientations for which the cracks are open; consequently, Eq. (5a) predicts shear dilatancy. Dilatancy under pure-shear stress is discussed in Appendix A.

In the original SCRAM theory (Dienes and Margolin, 1980; Dienes, 1996), material anisotropy was accounted for by keeping track of a number of crack orientations (normally 9), each with its own mean crack size. It is assumed here, as in ISOSCM (Addessio and Johnson, 1990), that the initial crack number density is isotropic ($N_0(\mathbf{n})=N_0$) and that the average crack size remains isotropic during loading ($\bar{c}(\mathbf{n},t)=\bar{c}(t)$), independent of the crack orientation. The intended use of the current model is for materials which do not exhibit strongly anisotropic damage and for stress states close to the hydrostat, such as in plate impact experiments, where the shear stress is often several orders of magnitude less than the pressure. With the assumption of an isotropic distribution of cracks, Addessio and Johnson (1990) found the analytical

expression for crack strains by carrying out the integration over all crack orientations. The shear crack strain is

$$\boldsymbol{\varepsilon}_{\mathrm{c}}^{\mathrm{s}}(\boldsymbol{\sigma},\bar{c}) = \frac{64\pi}{5G}\frac{1-v}{2-v}N_0\bar{c}^3\boldsymbol{\sigma}^{\mathrm{d}}, \tag{6}$$

where $\boldsymbol{\sigma}^{\mathrm{d}} \equiv \boldsymbol{\sigma} + p\mathbf{i}$ and $p \equiv -(\mathrm{tr}\,\boldsymbol{\sigma})/3$ are the stress deviator and pressure, respectively; $\mathbf{i}$ being the second-order identity tensor. It is noted that the explicit dependency of crack strain on time (t) has been replaced by the dependency on the mean crack size $\bar{c}$, which evolves with time.

In ISOSCM, the crack opening strain is zero if the pressure is positive ($p \geqslant 0$). When the pressure is negative ($p < 0$), the crack opening strain is found by carrying out the integration in Eq. (5a) over all crack orientations. The result can be written as

$$\boldsymbol{\varepsilon}_{\mathrm{c}}^{\mathrm{o}}(\boldsymbol{\sigma},\bar{c}) = \frac{64\pi}{15G}(1-v)N_0\bar{c}^3\left(\boldsymbol{\sigma} + \frac{1}{2}\mathrm{tr}\,(\boldsymbol{\sigma})\mathbf{i}\right)H[-p], \tag{7}$$

where H is the Heaviside function, which is one for a positive argument and zero when it is negative. The following well-known results (e.g., Batchelor, 1967) are useful in deriving the expressions for crack strains in Eqs. (6) and (7):

$$\int_{\Omega} \mathrm{d}\Omega = 2\pi, \tag{8a}$$

$$\int_{\Omega} \mathbf{n}\otimes\mathbf{n}\,\mathrm{d}\Omega = \frac{2\pi}{3}\mathbf{i}, \tag{8b}$$

$$\int_{\Omega} (\mathbf{n}\otimes\mathbf{n})\otimes(\mathbf{n}\otimes\mathbf{n})\,\mathrm{d}\Omega = \frac{2\pi}{15}((\mathbf{i}\otimes\mathbf{i}) + 2\mathbf{I}), \tag{8c}$$

where $\mathbf{I}$ is the symmetric fourth-order identity tensor having the components of $I_{ijkl} = (\delta_{ik}\delta_{jl} + \delta_{il}\,\delta_{jk})/2$, in terms of the Kronecker delta δ_{ij}.

The expression for the crack opening strain in Eq. (7) is consistent with crack mechanics for the stress states in which all three principal stresses have the same sign. Under that limitation, the sign of σ_n for an arbitrary crack orientation $\mathbf{n}$ is the same as the sign of the principal stresses. Therefore, all the cracks are closed when the pressure is positive ($p \geqslant 0$) and no crack opening strain can develop. Conversely, for a negative pressure ($p < 0$), all cracks are open and contribute to the crack opening strain, so the integration can be taken over all crack orientations. Eq. (7) is inconsistent with crack mechanics, however, when the principal stresses have mixed signs (e.g., pure-shear). For those stress states, cracks with some orientations are open while some others are closed, and the status of a crack (open or closed) cannot be determined by the sign of the pressure. In fact, regardless of the sign of the pressure, there is always a range of orientations, in the neighborhood of the direction of each tensile principal stress, in which cracks are open. The range depends on the relative magnitudes of the compressive and tensile principal stresses. Whether or not a crack orientation should be included in the integration in Eq. (5a) depends on its angles with the principal stresses; therefore, Eq. (7), based on the sign of the pressure, is not adequate. Indeed, Lewis and Schreyer (Lewis, 1991; Lewis and Schreyer, 1996) have found some anomalous results when Eq. (7) is applied to certain stress paths. They considered those stress states in detail and proposed a modification to Eq. (7). In their modification, when the principal stresses have mixed signs, the integration in Eq. (5a) is taken only inside the cone defining open cracks,

$$\boldsymbol{\varepsilon}_{\mathrm{c}}^{\mathrm{o}}(\boldsymbol{\sigma},\bar{c}) = \frac{16}{G}(1-v)N_0\bar{c}^3\left(\int_{\mathbf{n}\cdot\boldsymbol{\sigma}\mathbf{n}>0} (\mathbf{n}\otimes\mathbf{n})\otimes(\mathbf{n}\otimes\mathbf{n})\,\mathrm{d}\Omega\right)\boldsymbol{\sigma}. \tag{9}$$

For a given stress $\boldsymbol{\sigma}$, the range of integration over crack orientation is determined by $\mathbf{n}\cdot\boldsymbol{\sigma}\mathbf{n} > 0$. Let $\boldsymbol{\sigma} = \sum_{i=1,3}\sigma_i\mathbf{e}_i\otimes\mathbf{e}_i$ where σ_1, σ_2, σ_3 and $\mathbf{e}_1$, $\mathbf{e}_2$, $\mathbf{e}_3$ are the principal stresses and principal directions (unit

vectors), respectively. The principal stresses are sorted in descending order ($\sigma_1 \geqslant \sigma_2 \geqslant \sigma_3$) so that the material is said to be under pure-tension if $\sigma_3 > 0$, and under pure-compression if $\sigma_1 \leqslant 0$. The tension-compression stress states correspond to $\sigma_1 > 0 \geqslant \sigma_3$, i.e., the principal stresses have mixed signs; thus, Eq. (7) of Addessio and Johnson needs to be modified. The tension-compression case can be subdivided into two, according to the sign of σ_2, the intermediate principal stress. For $\sigma_2 \leqslant 0$, the crack normal can be taken as

$$\mathbf{n} = \cos\phi\mathbf{e}_1 + \sin\phi\sin\theta\mathbf{e}_2 + \sin\phi\cos\theta\mathbf{e}_3, \tag{10}$$

in terms of the azimuthal angle $\theta(0 \leqslant \theta \leqslant 2\pi)$ and declination angle ϕ $(0 \leqslant \phi \leqslant \pi/2)$ with respect to the principal stress axes. The open crack strain becomes

$$\boldsymbol{\varepsilon}_c^o(\boldsymbol{\sigma}, \bar{c}) = \frac{16}{G}(1-\nu)N_0\bar{c}^3\boldsymbol{\sigma}\int_0^{2\pi}\mathrm{d}\theta\int_0^{\phi_c}(\mathbf{n}\otimes\mathbf{n})\otimes(\mathbf{n}\otimes\mathbf{n})\sin\phi\,\mathrm{d}\phi, \tag{11}$$

with the limit of the declination angle

$$\phi_c = \cot^{-1}\sqrt{\chi_2\sin^2\theta + \chi_3\cos^2\theta}, \tag{12}$$

in which the parameters are defined as $\chi_i \equiv -\sigma_i/\sigma_1 \geqslant 0$, $i = 2, 3$. A similar expression can be derived for $\sigma_2 > 0$ (with ϕ being the angle with the $\mathbf{e}_3$ axis). In general the integration in Eq. (11) has to be carried out numerically. Lewis and Schreyer (1996) have performed such numerical integrations for a number of stress states and provided analytical fits to the numerical results.

2.1.1. Activated crack-opening strain

The modification by Lewis and Schreyer (Lewis, 1991; Lewis and Schreyer, 1996) for crack opening strain (i.e., Eq. (11)) is exact but requires numerical integration over crack orientations. This can be computationally intensive since the integration has to be performed at each time step when the stress state changes. Consequently, Lewis (1991) proposed using the activated crack-opening strain, which does not require numerical integrations, as an approximation to Eq. (11). The approximation is based on the numerical results of Eq. (11), and on the damage deactivation work of Hansen and Schreyer (1994, 1995). The main idea is to eliminate the contribution of the compressive principal stresses to the opening strain. The activated crack-opening strain is defined as a projection of the strain given in Eq. (7),

$$\boldsymbol{\varepsilon}_c^o(\boldsymbol{\sigma}, \bar{c}) = \frac{64\pi}{15G}(1-\nu)N_0\bar{c}^3\mathbf{P}^+\left(\mathbf{P}^d + \frac{5}{2}\mathbf{P}^{sp}\right)\mathbf{P}^+\boldsymbol{\sigma}, \tag{13a}$$

where the spherical and deviatoric projection operators are

$$\mathbf{P}^{sp} \equiv \frac{1}{3}(\mathbf{i}\otimes\mathbf{i}), \quad \mathbf{P}^d \equiv \mathbf{I} - \mathbf{P}^{sp}. \tag{13b, c}$$

Eq. (13a) reduces to Eq. (7) for the special cases when $\mathbf{P}^+ = \mathbf{I}$ and $p < 0$, or $\mathbf{P}^+ = \mathbf{O}$ and $p \geqslant 0$. The positive projection operator in Eq. (13a) is defined as

$$\mathbf{P}^+ \equiv \mathbf{Q}^+ \wedge \mathbf{Q}^+, \tag{14a}$$

where the cross composition of two symmetric second-order tensors, represented by the operator "$\wedge$", is defined as

$$\mathbf{A}\wedge\mathbf{B} \equiv \frac{1}{2}\left(A_{ik}B_{jl} + A_{il}B_{jk}\right)(\mathbf{e}_i\otimes\mathbf{e}_j\otimes\mathbf{e}_k\otimes\mathbf{e}_l). \tag{14b}$$

$\mathbf{Q}^+$ in Eq. (14a) is the positive spectral tensor of the stress, which is defined as

$$\mathbf{Q}^+ \equiv \sum_{i=1,3} H[\sigma_i]\mathbf{e}_i\otimes\mathbf{e}_i. \tag{15a}$$

The components of the positive projection operator are then

$$P^{+}_{ijkl} = \frac{1}{2}\left(Q^{+}_{ik}Q^{+}_{jl} + Q^{+}_{il}Q^{+}_{jk}\right). \tag{15b}$$

It follows from the definition that $\mathbf{Q}^{+}$ is a symmetric, second-order tensor. Our definition for the positive projection operator (Eqs. (14) and (15)) differs slightly from that in Hansen and Schreyer (1994, 1995) where the operator is defined as $\tilde{P}^{+}_{ijkl} \equiv Q_{ik}Q_{jl}$. The operator defined here possesses the minor symmetries, that is, $P^{+}_{ijkl} = P^{+}_{jikl} = P^{+}_{ijlk}$, which are absent in their definition ($\tilde{P}^{+}_{ijkl}$). However, the two definitions produce the same results when the projection operator is applied to symmetric (second-order) tensors, which is the case in the current work. The projected stress is then defined as

$$\boldsymbol{\sigma}^{+} \equiv \mathbf{P}^{+}\boldsymbol{\sigma} = (\mathbf{Q}^{+} \wedge \mathbf{Q}^{+})\boldsymbol{\sigma}. \tag{16a}$$

It follows that $\sigma^{+}_{ij} = (1/2)(Q^{+}_{ik}Q^{+}_{jl} + Q^{+}_{il}Q^{+}_{jk})\sigma_{kl} = Q^{+}_{ik}\sigma_{kl}Q^{+}_{lj}$, namely, $\boldsymbol{\sigma}^{+} = \mathbf{Q}^{+}\boldsymbol{\sigma}\mathbf{Q}^{+}$, in terms of second-order tensors.

Lewis (1991) compared the approximation in Eq. (13a) to the numerical results in Eq. (11) for a variety of stress states involving mixed signs of principal stresses, and found the approximation reasonable. Because no numerical integration is needed, Eq. (13a) is simpler and more efficient than Eq. (11); consequently, we will use it for the crack opening strain.

When a material is under pure tension, i.e., $\sigma_1 \geqslant \sigma_2 \geqslant \sigma_3 > 0$, we have $H[\sigma_i] = 1$, the positive spectral tensor becomes the second-order identity tensor ($\mathbf{Q}^{+} = \mathbf{i}$), and the positive projection operator reduces to the symmetric fourth-order identity ($\mathbf{P}^{+} = \mathbf{I}$). Consequently, $\boldsymbol{\sigma}^{+} = \boldsymbol{\sigma}$, and the crack opening strain given by Eq. (13a) reduces to Eq. (7). Similarly, when $0 \geqslant \sigma_1 \geqslant \sigma_2 \geqslant \sigma_3$, the material is under pure compression, and the positive spectral tensor and positive projection operator vanish ($\mathbf{Q}^{+} = \mathbf{o}$, $\mathbf{P}^{+} = \mathbf{O}$). Thus, there is no crack open strain ($\boldsymbol{\varepsilon}^{o}_{c}(\boldsymbol{\sigma}, \bar{c}) = \mathbf{o}$), again in agreement with Eq. (7). However, the current formulation, Eq. (13a), differs from Eq. (7) when the principal stresses are of mixed signs ($\sigma_1 > 0$ and $\sigma_3 \leqslant 0$). In terms of the principal stresses and principal directions,

$$\boldsymbol{\sigma} = \sum_{j=1,3} \sigma_j \mathbf{e}_j \otimes \mathbf{e}_j, \qquad \boldsymbol{\sigma}^{+} = \sum_{j=1,3} \langle \sigma_j \rangle \mathbf{e}_j \otimes \mathbf{e}_j, \tag{16b}$$

where the angled bracket again is the Macaulay bracket defined previously. Since $\sigma_1 > 0$ and $\sigma_3 \leqslant 0$, we have

$$\boldsymbol{\sigma} = \boldsymbol{\sigma}^{+} + \sum_{\alpha=N,3} \sigma_\alpha \mathbf{e}_\alpha \otimes \mathbf{e}_\alpha, \qquad N = \begin{cases} 2 & \text{if } \sigma_2 \leqslant 0, \\ 3 & \text{if } \sigma_2 > 0. \end{cases} \tag{16c}$$

That is, the projected stress ($\boldsymbol{\sigma}^{+}$) retains the tensile principal components of the stress ($\boldsymbol{\sigma}$), and removes the compressive ones. Thus, the positive projection operator ($\mathbf{P}^{+}$) in Eq. (13a) eliminates the contribution of the compressive principal stresses to the crack opening strain. This differs from Eq. (7) where either all or none of the principal stresses (tensile and compressive) contribute to the crack opening strain depending on the sign of pressure.

Finally, the total crack strain is obtained by substituting the expressions for crack shear strain and crack opening strain given by Eqs. (6) and (13a) into Eq. (4)

$$\boldsymbol{\varepsilon}_{c}(\boldsymbol{\sigma}, \bar{c}) = \beta^{e} N_0 \bar{c}^3 \left(\frac{3}{2-\nu} \boldsymbol{\sigma}^{d} + \mathbf{P}^{+} \left(\mathbf{P}^{d} + \frac{5}{2} \mathbf{P}^{sp} \right) \mathbf{P}^{+} \boldsymbol{\sigma} \right), \tag{17}$$

where $\beta^{e} \equiv 64\pi(1-\nu)/(15G)$ is a material constant depending on the elastic properties of the matrix (undamaged) material. Appendix A illustrates the use of the positive projection operator in calculating the crack strain for a pure-shear stress state (principal stresses of mixed signs).

2.2. Stress–strain relationship

In the absence of other inelastic mechanisms (such as plasticity, viscoelasticity, etc.), the total strain is the sum of the matrix strain $\boldsymbol{\varepsilon}_{\mathrm{m}}$ and crack strain $\boldsymbol{\varepsilon}_{\mathrm{c}}(\boldsymbol{\sigma}, \bar{c})$,

$$\boldsymbol{\varepsilon} = \boldsymbol{\varepsilon}_{\mathrm{m}} + \boldsymbol{\varepsilon}_{\mathrm{c}}(\boldsymbol{\sigma}, \bar{c}). \tag{18}$$

For an isotropic, linear elastic matrix material, the matrix strain is

$$\boldsymbol{\varepsilon}_{\mathrm{m}} = \mathbf{C}_{\mathrm{m}}\boldsymbol{\sigma}, \tag{19a}$$

$$\mathbf{C}_{\mathrm{m}} = \frac{1}{3K}\mathbf{P}^{\mathrm{sp}} + \frac{1}{2G}\mathbf{P}^{\mathrm{d}}, \tag{19b}$$

where $\mathbf{C}_{\mathrm{m}}$ and $K \equiv 2G(1+v)/(3(1-2v))$ are the compliance and bulk modulus of the matrix material, respectively. Substitution of Eqs. (17) and (19a) into Eq. (18) yields the stress–strain relationship:

$$\boldsymbol{\varepsilon} = \mathbf{C}_{\mathrm{m}}\boldsymbol{\sigma} + \beta^{\mathrm{e}} N_0 \bar{c}^3 \left(\frac{3}{2-v}\boldsymbol{\sigma}^{\mathrm{d}} + \mathbf{P}^{+}\left(\mathbf{P}^{\mathrm{d}} + \frac{5}{2}\mathbf{P}^{\mathrm{sp}}\right)\mathbf{P}^{+}\boldsymbol{\sigma} \right). \tag{20}$$

If the damage tensor $\mathbf{D}(\bar{c})$ is defined by $\boldsymbol{\varepsilon}_{\mathrm{c}}(\boldsymbol{\sigma}, \bar{c}) = \mathbf{D}(\bar{c})\boldsymbol{\sigma}$, then,

$$\boldsymbol{\varepsilon}(\boldsymbol{\sigma}, \bar{c}) = \mathbf{C}(\bar{c})\boldsymbol{\sigma}, \tag{21a}$$

$$\mathbf{C}(\bar{c}) = \mathbf{C}_{\mathrm{m}} + \mathbf{D}(\bar{c}). \tag{21b}$$

The current compliance of the damaged material, $\mathbf{C}(\bar{c})$, is the sum of the matrix compliance and the added compliance due to cracks. It follows from Eqs. (20) and (21) that the damage tensor is

$$\mathbf{D}(\bar{c}) = \beta^{\mathrm{e}} N_0 \bar{c}^3 \left(\frac{3}{2-v}\mathbf{P}^{\mathrm{d}} + \mathbf{P}^{+}\left(\mathbf{P}^{\mathrm{d}} + \frac{5}{2}\mathbf{P}^{\mathrm{sp}}\right)\mathbf{P}^{+} \right). \tag{22}$$

The expression for the damage tensor $\mathbf{D}(\bar{c})$ suggests the dimensionless crack density variable $d(\bar{c}) = N_0\bar{c}^3$ as a measure of damage in the material. The damage tensor $\mathbf{D}(\bar{c})$ is isotropic when the principal stresses are all tensile or all compressive. When the damage is isotropic, the response remains isotropic with the damaged shear and bulk moduli. Appendix B provides the detailed derivation of the damaged moduli as functions of the damage variable $d(\bar{c})$ for the cases where the principal stresses are of the same sign.

When the principal stresses have mixed signs, however, Eq. (22) predicts anisotropic damage with the directions of tensile principal stresses accumulating more damage than other directions. This is because cracks normal to any compressive principal stresses are closed; hence they cannot contribute to the normal component of the compliance in the directions of compressive principal stresses. Hansen and Schreyer (1994, 1995) defined this situation as damage deactivation. In their formulation, damage is only attributed to the "mode-I" (opening mode) loading; consequently, all damage will be deactivated under compressive loading. In the current formulation, however, the damage due to crack shearing is still accounted for even when the open damage is deactivated under compressive loading. For reactive materials, it has been argued (e.g., Dienes, 1982; Dienes, 1996; Bennett et al., 1998; Hackett and Bennett, 2000) that the frictional heating due to shear cracks can cause the formation of explosive hot spots. In fact, in Visco-SCRAM (Bennett et al., 1998; Hackett and Bennett, 2000) only shear damage is considered, and the volumetric response is taken as linear with the bulk modulus of the matrix material. That formulation is a special form of Eq. (22) for the pure-compressive stress states discussed earlier. For all other stress states where at least one of the principal stresses is tensile, the current formulation predicts "normal" damage, in addition to shear damage. An example of the pure-shear stress state is provided in Appendix A to illustrate the use of the positive projection operator in calculating the damage $\mathbf{D}(\bar{c})$.

Since the number density of cracks N_0 is assumed to remain constant during deformation, damage is accumulated only through increase of the average size $\bar{c}$. The evolution of damage $d(\bar{c})$ through the growth

of average crack size $\bar{c}$ is determined by the damage surface and the crack growth equation. We now develop the damage surface and the evolution equation for mean crack size. Damage increases when the stress state is outside the damage surface.

2.3. Damage surface

When the applied stress is sufficiently large, some cracks in the material can become unstable and grow in size. We assume here that the material accumulates additional damage if the crack with the average size $\bar{c}$ in some orientation is unstable, which occurs when the applied stress exceeds the critical value for that orientation. We also assume that cracks remain penny-shaped and are either open or closed, depending on the sign of the normal component of the remote traction on the crack surface. The Griffith instability criterion for a single crack with size $\bar{c}$ and normal $\mathbf{n}$ is, in terms of the energy-release rate,

$$F^{\mathbf{n}}(\boldsymbol{\sigma}, \mathbf{n}, \bar{c}) \equiv \frac{g(\boldsymbol{\sigma}, \mathbf{n}, \bar{c})}{2\gamma} - 1 \geqslant 0, \tag{23a}$$

where 2γ is the critical energy release rate with γ being the effective surface energy of the material. The energy-release rate for a penny-shaped crack under mixed-mode loading, which applies to both open cracks and closed cracks where interfacial friction is important, has been developed (e.g., Keer, 1966; Rice, 1984). The energy-release rate can be written as

$$g(\boldsymbol{\sigma}, \mathbf{n}, \bar{c}) = \frac{f(\boldsymbol{\sigma}, \mathbf{n})\bar{c}}{G} \frac{4}{\pi} \frac{(1-\nu)}{(2-\nu)}. \tag{23b}$$

The expression for the stress function $f(\boldsymbol{\sigma},\mathbf{n})$ depends on whether the crack is open (the normal component of traction is tensile) or closed (the normal component is compressive and controls the interfacial friction). For an open crack ($\sigma_n > 0$), both normal and shear stresses contribute to crack instability and the stress function $f(\boldsymbol{\sigma},\mathbf{n})$ is (Sack, 1946; Segedin, 1950; Keer, 1966)

$$f(\boldsymbol{\sigma}, \mathbf{n}) = (1 - \frac{\nu}{2})\sigma_n^2 + s_n^2, \tag{23c}$$

where the normal and shear components of the remote traction are $\sigma_n = \mathbf{n} \cdot \boldsymbol{\sigma}\mathbf{n}$ and $s_n = [\mathbf{n} \cdot \boldsymbol{\sigma}^2\mathbf{n} - (\mathbf{n} \cdot \boldsymbol{\sigma}\mathbf{n})^2]^{1/2}$, respectively. For a closed crack ($\sigma_n \leqslant 0$), the friction on the crack surface stabilizes the crack. If the Coulomb friction law is assumed, then the stress function $f(\boldsymbol{\sigma},\mathbf{n})$ is (Rice, 1984)

$$f(\boldsymbol{\sigma}, \mathbf{n}) = (s_n + \mu\sigma_n)^2 H(s_n + \mu\sigma_n), \tag{23d}$$

where μ is the static friction coefficient of the material and H is the Heaviside function defined earlier.

For a given crack size and stress state, the critical (most unstable) crack orientation, $\mathbf{n}^c$, maximizes the function $f(\boldsymbol{\sigma},\mathbf{n})$, hence the energy-release rate $g(\boldsymbol{\sigma}, \mathbf{n}^c, \bar{c})$. The crack with that orientation becomes unstable at the lowest applied stress and is defined here as the dominant crack. The damage function is defined by applying Eq. (23a) to the critical orientation $\mathbf{n}^c$,

$$F(\boldsymbol{\sigma}, \bar{c}) \equiv F^{\mathbf{n}}(\boldsymbol{\sigma}, \mathbf{n}^c, \bar{c}). \tag{24}$$

The damage surface is defined by $F(\boldsymbol{\sigma}, \bar{c}) = 0$, outside which (i.e., $F(\boldsymbol{\sigma}, \bar{c}) > 0$) the material accumulates additional damage and responses inelastically. We have found, for all possible stress states, the critical crack orientation, and determined the stress needed for the crack with that orientation to become unstable, hence, the damage surface (Zuo and Dienes, 2002, 2005). The following is a summary of the relevant results.

The damage surface $F(\boldsymbol{\sigma}, \bar{c}) = 0$ takes on one of the four different forms, depending on the stress state (the signs and relative magnitudes of the principal stresses). The four forms include tension (F^{o}), compression (F^{c}), combined opening and shear (F^{os}), and pure shear (F^{ps}).

2.3.1. $\sigma_1 \geqslant \sigma_2 \geqslant \sigma_3 \geqslant 0$

Material is in pure-tension; consequently, all cracks are open. The damage surface reduces to that of the Rankine maximum tensile criterion for brittle materials:

$$F^t(\boldsymbol{\sigma}, \bar{c}) \equiv \frac{\sigma_1}{S_{\rm cr}(\bar{c})/\sqrt{1-\nu/2}} - 1 = 0, \quad S_{\rm cr}(\bar{c}) \equiv \sqrt{\frac{\pi}{2}\frac{2-\nu}{1-\nu}\frac{G\gamma}{\bar{c}}}. \tag{25}$$

The critical crack normal is in the direction of maximum principal stress, $\mathbf{n}^c = \mathbf{e}_1$.

2.3.2. $0 \geqslant \sigma_1 \geqslant \sigma_2 \geqslant \sigma_3$

Material is in pure-compression; all cracks are closed and friction on crack surfaces plays an important role in resisting crack instability and hence increasing material strength. The damage surface becomes

$$F^{\rm c}(\boldsymbol{\sigma}, \bar{c}, \mu) \equiv \frac{(\sqrt{\mu^2+1}+\mu)\sigma_1 - (\sqrt{\mu^2+1}-\mu)\sigma_3}{2S_{\rm cr}(\bar{c})} - 1 = 0. \tag{26}$$

This surface coincides with the Mohr–Coulomb surface for a brittle material with the cohesion of the material taken as $S_{\rm cr}(\bar{c})$, which decreases monotonically during damage accumulation as the mean crack size ($\bar{c}$) increases. The damage surface based on the instability condition for the dominant crack provides a justification for the Mohr–Coulomb surface for brittle materials and the means to relate the cohesion constant to the defects in the materials. The angle between the critical normal ($\mathbf{n}^c$) and $\mathbf{e}_3$, the direction of largest compressive principal stress, is $\theta^c \equiv \tan^{-1}(\sqrt{\mu^2+1}+\mu)$, which implies that as the friction coefficient μ increases, the critical crack plane becomes increasingly parallel to the largest compressive stress direction (axial splitting).

2.3.3. $\sigma_1 > 0$ and $\sigma_3 < 0$

Material is in tension-compression; cracks with certain orientations are open and the rest are closed. The damage surface depends on the relative magnitudes of the principal stresses. Let $r \equiv \sigma_3/\sigma_1 < 0$ denote the stress biaxiality in the $\sigma_1 - \sigma_3$ plane. Then,

2.3.3.1. $-1 \leqslant r < 0$ (i.e., $\sigma_1 \geqslant -\sigma_3$)

- **a.** $-(1-\nu) \leqslant r < 0$. The damage surface and the critical crack orientation are the same as case 2.3.1 (pure-tension state of stress).
- **b.** $-1 \leqslant r < -(1-\nu)$. The critical crack is in combined tensile and shear loading (all three modes are present, e.g., Rice, 1984; Kachanov, 1993). The damage surface has an elliptic cross section,

$$F^{\rm os}(\boldsymbol{\sigma}, \bar{c}) \equiv \frac{\left(\frac{2}{\nu}-1\right)\left(\frac{\sigma_1+\sigma_3}{2}\right)^2 + \left(\frac{\sigma_1-\sigma_3}{2}\right)^2}{S_{\rm cr}^2(\bar{c})} - 1 = 0. \tag{27}$$

The angle of the critical crack normal with the $\mathbf{e}_1$ axis is

$$\theta^\circ = \frac{1}{2}\cos^{-1}\left\{\left(\frac{2}{\nu}-1\right)\frac{1+r}{1-r}\right\}. \tag{28}$$

2.3.3.2. $r \leqslant -1$ (i.e., $\sigma_1 \leqslant -\sigma_3$)

- **a.** $r < -(\sqrt{\mu^2+1}+\mu)^2$. The damage surface and the critical crack orientation are the same as 2.3.2 the pure-compression state of stress.
- **b.** $-(\sqrt{\mu^2+1}+\mu)^2 \leqslant r \leqslant -1$. The critical crack is a pure-shear crack ($\sigma_n = 0$) and the damage surface has a hyperbolic cross section,

$$F^{ps}(\boldsymbol{\sigma},\bar{c}) = -\frac{\sigma_1\sigma_3}{S_{cr}^2(\bar{c})} - 1 = 0. \tag{29}$$

The angle of the critical normal with the $\mathbf{e}_1$ (tensile) axis is $\theta^s = \tan^{-1}(1/\sqrt{-r})$.

The damage surface $F(\boldsymbol{\sigma},\bar{c}) = 0$ (Eqs. (25)–(27) and (29)) involves only the current stress (the maximum and minimum principal stresses, σ_1 and σ_3, respectively) and the mean crack size $\bar{c}$. The intermediate principal stress (σ_2) has no effect on the damage surface. This is a consequence of the instability condition (i.e., Eq. (23a)), which is independent of the stress components in the plane of the crack. The damage surface for a triaxial stress state is illustrated in Fig. 1. The applied axial (σ_{11}) and radial ($\sigma_{33} = \sigma_{22}$) stresses are normalized with respect to the tensile-damage threshold of the material ($S_{\alpha\alpha} \equiv \sigma_{\alpha\alpha}/P_{cr}^t; P_{cr}^t = S_{cr}(\bar{c})/\sqrt{1-\nu/2}$), which decreases with crack size $\bar{c}$ (Eq. (25)). The surface captures the main features of brittle behavior under triaxial loadings. For example, the compressive threshold stress is much larger than the tensile threshold stress (the former increases significantly with pressure and friction coefficient while the latter is independent of friction). The damage surface is also similar to the fracture surfaces for brittle materials that other researchers have proposed and are supported by experimental data (McClintock and Walsh, 1962; Keer, 1966; Alpa, 1984). Those researchers considered brittle materials containing isotropically distributed cracks and assumed that fracture occurs when crack with the worst (critical) orientation becomes unstable.

Fig. 2 is a comparison of the new damage surface and the damage surface used in ISOSCM, which was based on averaging the crack instability condition over all crack orientations. The state of stress is taken to be triaxial (uniform lateral confinement). In ISOSCM, the damage surface was given in terms of the pressure and von Mises (shear) stress ($\tau \equiv \sqrt{(3/2)\boldsymbol{\sigma}^d : \boldsymbol{\sigma}^d}$). Consequently, we have transformed the new damage surface from the principal stress space into the plane of normalized pressure and shear

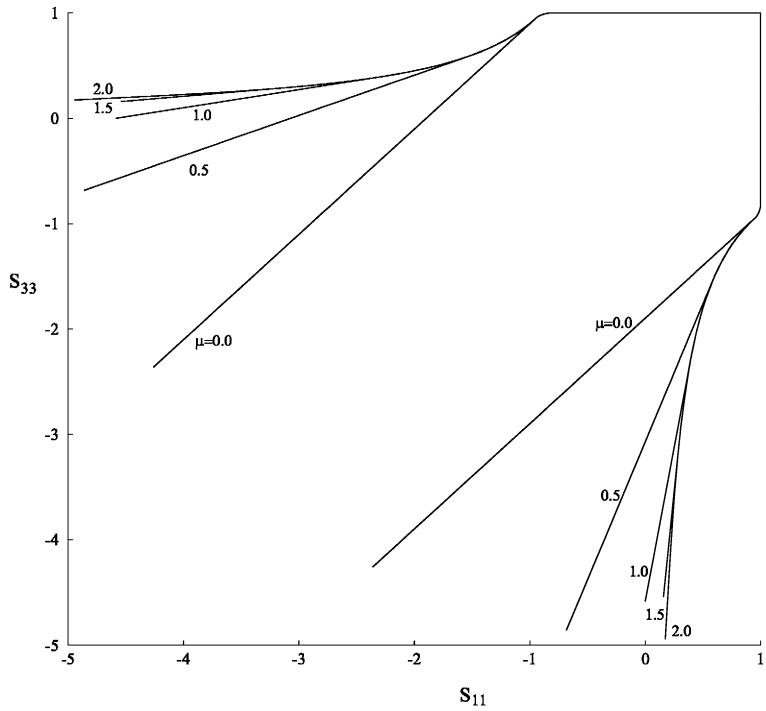

Fig. 1. Damage surface for a brittle material under triaxial loading for values of the friction coefficient (μ) ranging from 0 to 2.0.

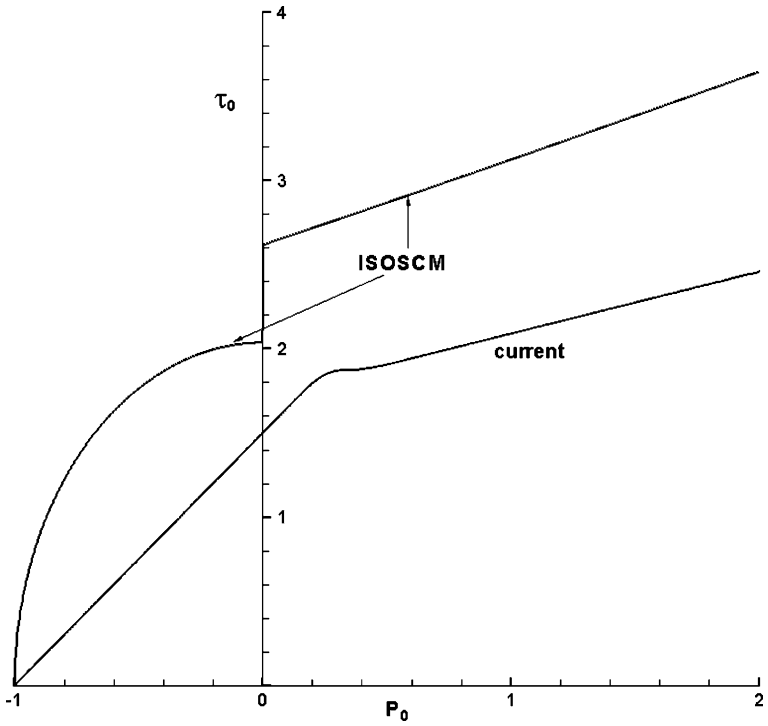

Fig. 2. Comparison of the current damage surface and that used in ISOSCM (Addessio and Johnson, 1990).

($P_0 \equiv p/P^t_{cr}; \tau_0 \equiv \tau/P^t_{cr}$). In this plane, the only material constants that affect the damage surfaces are the Poisson's ratio ν and friction coefficient μ. The same set of material constants ($\nu = 0.25$ and $\mu = 0.2$) was used in generating the two surfaces. Both surfaces predict the same value when the material is under isotropic (hydrostatic) tension, since in this case every orientation is equally critical and hence the two approaches are identical. Both approaches predict no damage evolution (crack growth) under hydrostatic compression ($\tau = 0$), consistent with crack mechanics. For a non-isotropic stress state ($\tau > 0$), the current approach predicts less shear before additional damage accrues than the previous approach. This is consistent with the assumptions that damage grows when the crack with any (the critical) orientation is unstable while the previous approach assumes damage can grow only when the crack with some averaged orientation is unstable. The most important difference is that the new damage surface based on the critical orientation is continuous, whereas the surface based on orientation-averaging has a jump as the pressure changes sign. The jump in the damage surface, an artifact of averaging the instability condition over all crack orientations, is unphysical. It has been shown (Lewis, 1991; Lewis and Schreyer, 1996) that the jump causes energy creation under certain cyclic load paths and renders the model thermodynamically inconsistent. Note that the stresses in Figs. 1 and 2 have been normalized and hence are non-dimensional.

2.4. Damage evolution via crack growth

For a stress state outside the damage surface $F(\boldsymbol{\sigma}, \bar{c}) > 0$, the material will accumulate additional damage via growth of the mean crack size. Rajendran and Grove (1996) derived a crack growth law based on the equation of motion for the crack tip for a single crack (Kanninen and Popelar, 1985; Freund, 1972, 1990). The result is that the crack growth rate is a function of the applied energy-release rate. The crack growth

law used in the current work is similar to that by Rajendran and Grove, but here we use the energy-release rate for the crack with the critical orientation (the dominant crack) to calculate the growth rate. This is consistent with the derivation of the current damage surface, which is based on the instability of cracks with the critical orientation. The crack growth law is

$$\dot{\bar{c}} = \dot{c}_{\max}\left\langle 1 - \frac{2\gamma}{g(\boldsymbol{\sigma}, \mathbf{n}^c, \bar{c})}\right\rangle, \tag{30}$$

where $\dot{c}_{\max}$ is the terminal speed for crack growth. The terminal speed $\dot{c}_{\max}$ is either the shear wave speed of the matrix for closed cracks, or the Rayleigh wave speed C_R for open cracks, which is only slightly less than the shear wave speed (e.g., $C_R = 0.93C_s$, for a Poisson's ratio of $v = 0.3$, Meyers, 1994). The choice depends on whether the crack with the critical orientation is open ($\sigma_n(\mathbf{n}^c) \equiv \mathbf{n}^c \cdot \boldsymbol{\sigma}\mathbf{n}^c > 0$) or closed ($\sigma_n(\mathbf{n}^c) \leqslant 0$). Recall that γ is the effective surface energy of the material, and therefore 2γ is the critical energy release rate for a penny-shaped crack (e.g., Rice, 1984). It follows that the crack growth speed asymptotically approaches the terminal speed as the energy release rate increases.

Since the damage function is based on the energy release rate for the critical orientation, we can conveniently relate the crack growth to the damage function. Substituting Eqs. (23a) and (24) into Eq. (30) yields an expression for the rate of growth of mean crack radius in terms of the damage function $F(\boldsymbol{\sigma}, \bar{c})$:

$$\frac{\dot{\bar{c}}}{\dot{c}_{\max}} = 1 - \frac{1}{1 + \langle F(\boldsymbol{\sigma}, \bar{c})\rangle}. \tag{31}$$

The crack growth rate is zero when the stress state is inside or on the damage surface ($F(\boldsymbol{\sigma}, \bar{c}) \leqslant 0$), and increases monotonically with $F(\boldsymbol{\sigma}, \bar{c})$, the distance of the stress state from the damage surface, when the stress state is outside the surface ($F(\boldsymbol{\sigma}, \bar{c}) > 0$). Since $F(\boldsymbol{\sigma}, \bar{c}) = 0$ defines the damage surface, the value of $F(\boldsymbol{\sigma}, \bar{c})$ represents a measure of the distance of the stress state from the damage surface. The proposed rate-dependent damage evolution law (Eq. (31)) is analogous to the classical over-stress model frequently used in rate-dependent plasticity (e.g., Lubliner, 1990). The need for including the rate-dependence in plasticity, especially in the context of modeling material responses involving softening and localization, has long been recognized (e.g., Addessio and Johnson, 1993). The rate-effects provide a length-scale which is absent in a rate-independent model, but is needed in a well-posed initial/boundary value problem.

In the original formulation of ISOSCM, two approaches were considered for the damage growth rate. In the rate-independent approach, the crack growth rate is solved for by requiring that the material state remain on the damage surface (similar to using the consistency condition in the rate-independent plasticity formulations). It was found, however, that for crack sizes smaller than a critical value, the approach unphysically predicts crack healing (negative growth rate). Consequently, a rate-dependent approached was used in ISOSCM, in which the crack growth rate was assumed to be an exponential function of the distance of the stress state exceeding the damage surface. Numerical calculations of a single cell under a prescribed uniaxial strain path suggest the rate-dependent approach was reasonable. However, no physical justification was provided for that assumption on the crack growth rate. The current formulation (Eq. (31)) is a modification to the rate-dependent approach in the original formulation. Since the damage function used here is directly related to the energy release rate for the critical crack orientation, it provides some physical justification for using the rate-dependent over-stress model for damage evolution.

In computer calculations, for a time step which gives the stress state inside or on the damage surface, $F(\boldsymbol{\sigma}, \bar{c}) \leqslant 0$, it follows from Eq. (31) that there is no damage accumulation during the step and the response is elastic. However, if the stress state is outside the surface ($F(\boldsymbol{\sigma}, \bar{c}) > 0$), additional damage accumulates according to the evolution equation (Eq. (31)), and the response is inelastic. The detailed algorithm for advancing the damage is given next.

3. Numerical algorithms

The rate form of the constitutive equation (Eq. (21)) may be written as

$$\dot{\boldsymbol{\varepsilon}} = \dot{\boldsymbol{\varepsilon}}_{\mathrm{m}} + \dot{\boldsymbol{\varepsilon}}_{\mathrm{c}} = \dot{\boldsymbol{\varepsilon}}_{\mathrm{m}} + \left(\dot{\boldsymbol{\varepsilon}}_{\mathrm{c}}^{d} + \dot{\boldsymbol{\varepsilon}}_{\mathrm{c}}^{\mathrm{gr}}\right) = \mathbf{C}_{\mathrm{m}}\dot{\boldsymbol{\sigma}} + \left(\mathbf{D}(\bar{c})\dot{\boldsymbol{\sigma}} + \frac{\partial \mathbf{D}(\bar{c})}{\partial \bar{c}}\dot{\bar{c}}\boldsymbol{\sigma}\right). \tag{32}$$

That is, the total strain rate is the sum of the matrix strain rate ($\dot{\boldsymbol{\varepsilon}}_{\mathrm{m}} = \mathbf{C}_{\mathrm{m}}\dot{\boldsymbol{\sigma}}$) and the crack strain rate $\dot{\boldsymbol{\varepsilon}}_{\mathrm{c}}$. The crack strain rate is made up of an elastic contribution due to the rate of change in stress ($\dot{\boldsymbol{\varepsilon}}_{\mathrm{c}}^{d} = \mathbf{D}(\bar{c})\dot{\boldsymbol{\sigma}}$) and an inelastic part ($\dot{\boldsymbol{\varepsilon}}_{i} = \dot{\boldsymbol{\varepsilon}}_{\mathrm{c}}^{\mathrm{gr}} = \dot{\bar{c}}(\partial \mathbf{D}(\bar{c})/\partial \bar{c})\boldsymbol{\sigma}$), due to damage accumulation (crack growth). It is emphasized here that the elastic strain rate includes both the matrix strain rate and a part of the crack strain rate, namely, $\dot{\boldsymbol{\varepsilon}}_{e} = \dot{\boldsymbol{\varepsilon}}_{\mathrm{m}} + \dot{\boldsymbol{\varepsilon}}_{\mathrm{c}}^{d}$. This was not included in ISOSCM (Addessio and Johnson, 1990). It is interesting to observe that the inelastic strain rate, which is due to crack growth, is like a viscous strain rate in that it is proportional to the stress tensor, not its rate.

In a computer program, the strain rate is often obtained from the momentum equation and one needs to find the stress rate and the rate of damage growth. To that end, the constitutive laws of Eqs. (31) and (32) are recast as

$$\dot{\boldsymbol{\sigma}} = (\mathbf{C}_{\mathrm{m}} + \mathbf{D}(\bar{c}))^{-1}(\dot{\boldsymbol{\varepsilon}} - \dot{\boldsymbol{\varepsilon}}_{\mathrm{c}}^{\mathrm{gr}}), \tag{33a}$$

$$\dot{\boldsymbol{\varepsilon}}_{\mathrm{c}}^{\mathrm{gr}} = (3\dot{\bar{c}}/\bar{c})\mathbf{D}(\bar{c})\boldsymbol{\sigma}, \tag{33b}$$

$$\dot{\bar{c}} = \dot{c}_{\max}\left(1 - \frac{1}{1 + \langle F(\boldsymbol{\sigma}, \bar{c})\rangle}\right), \tag{33c}$$

where Eq. (22) for the damage tensor has been used to compute $\partial \mathbf{D}(\bar{c})/\partial \bar{c}$. It follows from Eq. (33a) that $(\dot{\boldsymbol{\varepsilon}} - \dot{\boldsymbol{\varepsilon}}_{\mathrm{c}}^{\mathrm{gr}})$ is the elastic strain rate ($\dot{\boldsymbol{\varepsilon}}_{e}$) and $(\mathbf{C}_{m} + \mathbf{D}(\bar{c}))^{-1}$ is the instantaneous elasticity tensor of the damaged material. Eq. (33a) is a special form of the general result in Dienes (1996), which is based on the superposition of strain rates, rather than the superposition of strains adopted here. We have shown that the two approaches yield the same result.

With the damage tensor $\mathbf{D}(\bar{c})$ defined in Eq. (22), the rate equations for stress and mean crack size can be integrated numerically. Consider a time step $\Delta t = t^{n+1} - t^{n}$ with the total strain increment given by $\Delta\boldsymbol{\varepsilon} = \dot{\boldsymbol{\varepsilon}}\Delta t$. Suppose the stress and crack size at the beginning of the time step are given by $(\boldsymbol{\sigma}^{n}, \bar{c}^{\mathrm{n}})$. The goal of the algorithm is to find the stress and crack size at the end of the time step $(\boldsymbol{\sigma}^{n+1}, \bar{c}^{n+1})$. We will now develop an implicit algorithm for updating the material state $(\boldsymbol{\sigma}^{n+1}, \bar{c}^{n+1})$. An implicit integration algorithm offers the advantage of placing no additional stability constraint on the size of the time step, which could be an issue for the explicit algorithm (as we will see later).

Eliminating the inelastic (crack growth) strain rate ($\dot{\boldsymbol{\varepsilon}}_{\mathrm{c}}^{\mathrm{gr}}$) in Eqs. (33a) and (33b) results in an evolution equation for the stress in terms of stress and crack size. Applying the backward Euler integration scheme to that evolution equation gives the final stress as

$$\boldsymbol{\sigma}^{n+1}(\bar{c}^{n+1}) = \left(\mathbf{I} + 3\left(1 - \frac{\bar{c}^{n}}{\bar{c}^{n+1}}\right)(\mathbf{C}_{m} + \mathbf{D})^{-1}\mathbf{D}\right)^{-1}\left(\boldsymbol{\sigma}^{n} + (\mathbf{C}_{\mathrm{m}} + \mathbf{D})^{-1}\Delta\boldsymbol{\varepsilon}\right), \tag{34}$$

where the relationship $\dot{\bar{c}}\Delta t = \bar{c}^{n+1} - \bar{c}^{n}$ has been used, and the dependency of $\mathbf{D}(\bar{c}^{n+1})$ on $\bar{c}^{n+1}$ has been dropped for compactness. With the material state at the beginning of the step $(\boldsymbol{\sigma}^{n}, \bar{c}^{n})$ and the strain increment $(\Delta\boldsymbol{\varepsilon})$ given and fixed, the final stress $\boldsymbol{\sigma}^{n+1}$ is a function of the final crack size $\bar{c}^{n+1}$ only. The final crack size $\bar{c}^{n+1}$ is solved with the following procedure. First, define the trial state by assuming the step is elastic, i.e., there is no crack growth during the step, $\bar{c}^{\mathrm{tr}} = \bar{c}^{n}$:

$$\boldsymbol{\sigma}^{\mathrm{tr}} \equiv \boldsymbol{\sigma}^{n} + (\mathbf{C}_{\mathrm{m}} + \mathbf{D}(\bar{c}^{n}))^{-1}\Delta\boldsymbol{\varepsilon}. \tag{35}$$

If both the stress state at the beginning of the time step and the trial stress state are inside or on the damage surface, i.e., $F(\boldsymbol{\sigma}^n, \bar{c}^n) \leqslant 0$ and $F(\boldsymbol{\sigma}^{\mathrm{tr}}, \bar{c}^n) \leqslant 0$, then the step is indeed purely elastic. In this case, the trial state is the final solution, $\bar{c}^{n+1} = \bar{c}^{\mathrm{tr}}$, $\boldsymbol{\sigma}^{n+1} = \boldsymbol{\sigma}^{\mathrm{tr}}$. Otherwise, the step involves crack growth and a correction to the trial state is needed. Depending on whether the trial state is inside or outside the damage surface, one of the following two algorithms is used:

A. $F(\boldsymbol{\sigma}^{\mathrm{tr}}, \bar{c}^n) > 0$. The trial state is outside the damage surface, as illustrated in Fig. 3. Applying the central difference scheme (the trapezoidal rule) to the evolution equations for the crack size (Eq. (33c)) yields

$$\frac{\bar{c}^{n+1} - \bar{c}^n}{\dot{c}_{\max}\Delta t} - \left(1 - \frac{1}{1 + \frac{1}{2}\left(F(\boldsymbol{\sigma}^{n+1}, \bar{c}^{n+1}) + \langle F(\boldsymbol{\sigma}^n, \bar{c}^n)\rangle\right)}\right) = 0. \tag{36}$$

With $\boldsymbol{\sigma}^{n+1}$ given by Eq. (34) as a function of $\bar{c}^{n+1}$ only, Eq. (36) is a nonlinear equation for $\bar{c}^{n+1}$, which can be solved by an iterative method, using the trail state $(\boldsymbol{\sigma}^{\mathrm{tr}}, \bar{c}^n)$ as the starting state for the iteration. During the iteration, the solution is constrained to be outside the damage surface,

$$F(\boldsymbol{\sigma}^{n+1}, \bar{c}^{n+1}) > 0. \tag{37}$$

Once $\bar{c}^{n+1}$ is solved, the final stress can be calculated from Eq. (34).

B. $F(\boldsymbol{\sigma}^{\mathrm{tr}}, \bar{c}^n) \leqslant 0$ and $F(\boldsymbol{\sigma}^n, \bar{c}^n) > 0$. The step starts with the stress state outside the surface, and ends with the state possibly inside the surface, as illustrated in Fig. 4. The material is unloaded during the step, but cracks still grow during the first portion of the time step when the stress state is outside the damage surface. For the rest of the time step, the stress state remains inside the damage surface and the material unloads elastically. Physical justification for possible crack growth during unloading is that, due to inertia, crack arrest does not occur instantaneously; rather, it takes a finite amount of time for a dynamically growing crack to decelerate into an equilibrium state. We first find the equilibrium state $(\boldsymbol{\sigma}^{\mathrm{eq}}, \bar{c}^{\mathrm{eq}})$ and the fraction of the time step $(\Delta t^{\mathrm{eq}} < \Delta t)$ needed for the crack growth to reach the equilibrium $(\dot{\bar{c}}^{\mathrm{eq}} = 0)$. According to Eq. (31), the equilibrium is reached when the stress state reaches the damage surface from outside. This is done by first applying the discretized evolution equations (Eqs. (33)) over the sub-step Δt^{eq}, and requiring the equilibrium state to be on the damage surface $(F(\boldsymbol{\sigma}^{\mathrm{eq}}, \bar{c}^{\mathrm{eq}}) = 0)$,

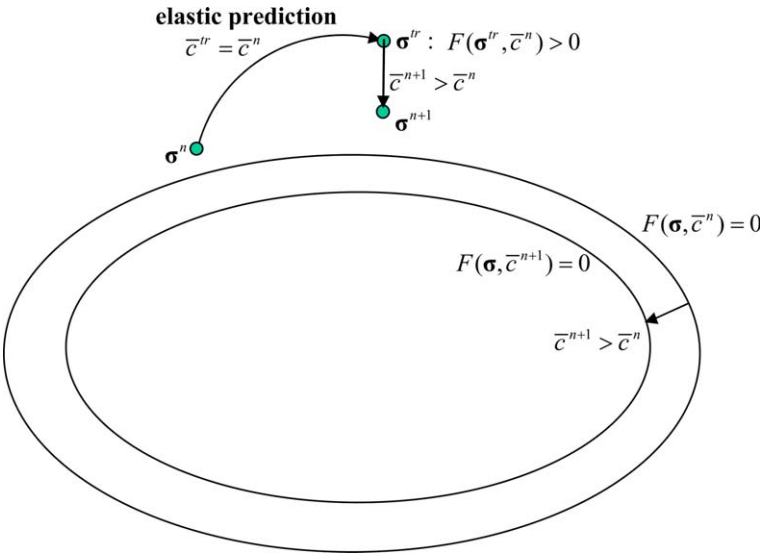

Fig. 3. Sketch of the prediction-correction algorithm for the step with $F(\boldsymbol{\sigma}^{\mathrm{tr}}, \bar{c}^n) > 0$.

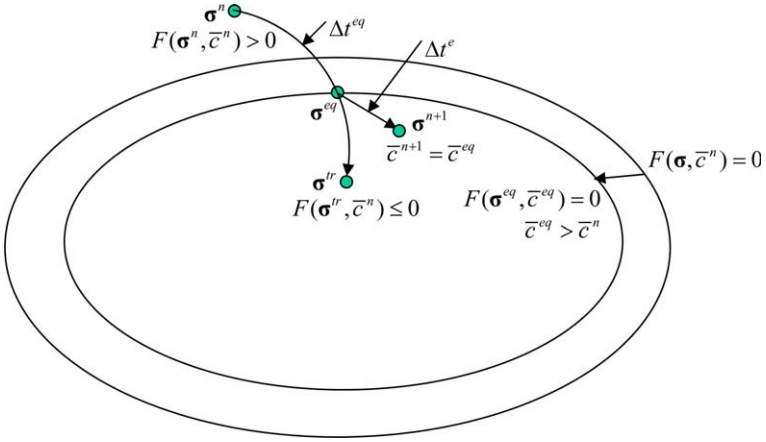

Fig. 4. Sketch of the numerical algorithm with $F(\boldsymbol{\sigma}^{\mathrm{tr}},\bar{c}^n)\leqslant 0$ and $F(\boldsymbol{\sigma}^n,\bar{c}^n)>0$.

$$\boldsymbol{\sigma}^{\mathrm{eq}}(\bar{c}^{\mathrm{eq}},\Delta t^{\mathrm{eq}})=\left(\mathbf{I}+3\left(1-\frac{\bar{c}^n}{\bar{c}^{\mathrm{eq}}}\right)(\mathbf{C}_m+\mathbf{D})^{-1}\mathbf{D}\right)^{-1}\left(\boldsymbol{\sigma}^n+\Delta t^{\mathrm{eq}}(\mathbf{C}_{\mathrm{m}}+\mathbf{D})^{-1}\dot{\boldsymbol{\varepsilon}}\right), \tag{38}$$

$$\bar{c}^{\mathrm{eq}}=\bar{c}^n+\left(1-\frac{1}{1+F(\boldsymbol{\sigma}^n,\bar{c}^n)/2}\right)\dot{c}_{\max}\Delta t^{\mathrm{eq}}, \tag{39}$$

$$F(\boldsymbol{\sigma}^{\mathrm{eq}},\bar{c}^{\mathrm{eq}})=0, \tag{40}$$

where $\mathbf{D}=\mathbf{D}(\bar{c}^{\mathrm{eq}})$, a function of $\bar{c}^{\mathrm{eq}}$. Since $F(\boldsymbol{\sigma}^n,\bar{c}^n)$ is known, Δt^{eq} can be easily solved from in Eq. (39), in terms of $\bar{c}^{\mathrm{eq}}$:

$$\Delta t^{\mathrm{eq}}(\bar{c}^{\mathrm{eq}})=\frac{\bar{c}^{\mathrm{eq}}-\bar{c}^n}{\dot{c}_{\max}}\left(\frac{2}{F(\boldsymbol{\sigma}^n,\bar{c}^n)}+1\right). \tag{41}$$

Substituting Δt^{eq} into (38) yields the equilibrium stress $\boldsymbol{\sigma}^{\mathrm{eq}}$ as a function of the equilibrium crack size $\bar{c}^{\mathrm{eq}}$ only; consequently, Eq. (40) becomes a nonlinear scalar equation for $\bar{c}^{\mathrm{eq}}$, which can be solved by an algorithm similar to the one used to solve Eq. (36).

The rest of the step is elastic unloading with the elastic strain increment given by $\Delta\boldsymbol{\varepsilon}^{\mathrm{e}}=(\Delta t-\Delta t^{\mathrm{eq}})\dot{\boldsymbol{\varepsilon}}$. The final crack size and stress are

$$\bar{c}^{n+1}=\bar{c}^{\mathrm{eq}}, \tag{42a}$$

$$\boldsymbol{\sigma}^{n+1}=\boldsymbol{\sigma}^{\mathrm{eq}}+\left(\mathbf{C}_{\mathrm{m}}+\mathbf{D}(\bar{c}^{n+1})\right)^{-1}\Delta\boldsymbol{\varepsilon}^{\mathrm{e}}. \tag{42b}$$

In deriving the discretized evolution equations for the crack size (Eqs. (36) and (39)), the central difference scheme has been used, rather than the backward Euler scheme. In addition to the accuracy consideration (the central difference is a second-order scheme while the backward Euler is first-order), there are two practical reasons for the choice. (1) Because $F(\boldsymbol{\sigma}^{\mathrm{eq}},\bar{c}^{\mathrm{eq}})=0$ at the equilibrium state, using the backward Euler scheme would erroneously prevent crack growth over the sub-step Δt^{eq}. (2) For some test problems with large time steps, our iterative method using the Euler backward scheme converges very slowly (or even fails to converge sometimes) whereas the method converges rapidly using the central difference scheme.

In high-rate applications such as chemical explosions or high-velocity mechanical impact problems, explicit analysis codes can often be used effectively with small time steps. In that situation, it is often more efficient and simpler to use the explicit algorithm to integrate the evolution equations. In the explicit

algorithm, the crack growth and the inelastic strain due to crack growth are determined from the material state (i.e., stress and crack size) at the beginning of the time step (t_n):

$$\Delta\bar{c} = \dot{c}_{\max}\Delta t\left(1 - \frac{1}{1 + \langle F(\boldsymbol{\sigma}^n, \bar{c}^n)\rangle}\right), \tag{43a}$$

$$\Delta\boldsymbol{\varepsilon}_c^{\mathrm{gr}} = (3\Delta\bar{c}/\bar{c}^n)\mathbf{D}(\bar{c}^n)\boldsymbol{\sigma}^n. \tag{43b}$$

The stress and crack size at the end of the step are then

$$\bar{c}^{n+1} = \bar{c}^n + \Delta\bar{c}, \tag{44a}$$

$$\boldsymbol{\sigma}^{n+1} = \boldsymbol{\sigma}^n + (\mathbf{C}_{\mathrm{m}} + \mathbf{D}(\bar{c}^n))^{-1}(\Delta\boldsymbol{\varepsilon} - \Delta\boldsymbol{\varepsilon}_c^{\mathrm{gr}}). \tag{44b}$$

Because no iterations are need, the explicit algorithm is simpler and faster than the implicit algorithm discussed earlier. However, the explicit algorithm often poses a strict limit on the size of the time step. Fig. 5 compares the model predictions using the implicit and explicit algorithms with 4 different time steps (from 0.01 ns to 10 ns). The loading is uniaxial strain with a strain rate of $\dot{\varepsilon}_{11} = 10^5\ \mathrm{s}^{-1}$, and the model material is silicon carbide (SiC) ceramic. The material constants are taken from ISOSCM (Addessio and Johnson, 1990) and reproduced in Table 1 for convenience. As the time step is reduced, both the implicit and explicit algorithms converge to the same result (the curve in the middle with $\Delta t \leqslant 0.1$ ns). It is also shown that the implicit algorithm gives a more accurate result for large time steps. For $\Delta t = 10$ ns (corresponding to a strain increment of $\Delta\varepsilon_{11} = 10^{-3}$), the explicit algorithm produces severe oscillations.

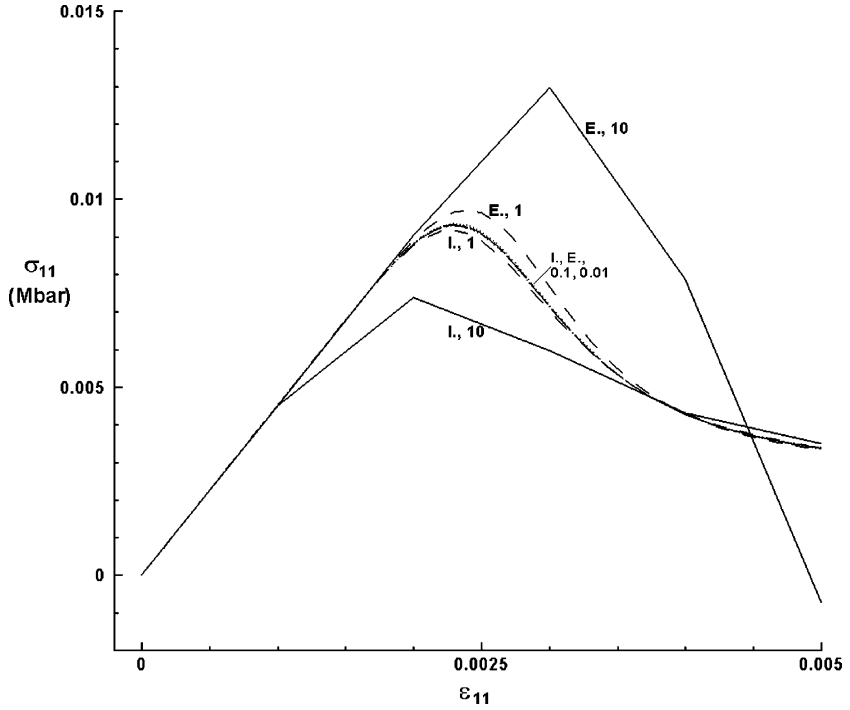

Fig. 5. Comparison of the predicted stress–strain responses using implicit (I) and explicit (E) algorithms with 4 time-step sizes: 10 ns, 1 ns, 0.1 ns, and 0.01 ns.

Table 1
Material constants for SiC ceramic (Addessio and Johnson, 1990)

ρ (g/cm^3), mass density	3.177
G (Mbar), shear modulus	1.869
ν, Poisson's ratio	0.16
$\bar{c}_0$ (cm), initial crack size	$14. \times 10^{-4}$
N_0 (cm^{-3}), crack number density	1.0×10^5
γ (Mbar cm), surface energy	1.0×10^{-8}
μ, friction coefficient	0.26

4. Numerical examples

To illustrate the features of the proposed model, several standard load paths (hydrostatic, uniaxial strain, uniaxial stress, and pure-shear) have been simulated with the stand-alone driver program. The results are given in Figs. 6–10. The model material is the same SiC ceramic used in Section 3.

Fig. 6 shows the stress response (Fig. 6a) and the crack size evolution (Fig. 6b) to a hydrostatic (isotropic, $\boldsymbol{\varepsilon} = \varepsilon_{11}\mathbf{i}$, $\boldsymbol{\sigma} = -P\mathbf{i}$), cyclic loading, with a strain rate $\dot{\varepsilon}_{11} = 10^5\ \mathrm{s}^{-1}$. The material is initially stress-free (point **A**) and is first loaded up to a tensile strain of 0.01 (**C**), then unloaded back to zero strain (**A**) and reverse loaded (compression) to a strain of $\varepsilon_{11} = -0.0005$ (**D**), and finally reloaded to a tensile strain of 0.0195 (**E**). The bold-faced letters used in this section refer to the various points labeled in the figures. The evolution of the damage surface is superimposed on the stress–strain response (Fig. 6a). The initial loading path (**A**–**A**′–**B**–**C**) begins with an elastic response **A**–**A**′, with the slightly damaged modulus corresponding to the initial crack size $\bar{c}_0 = 14\ \mu\mathrm{m}$. When the stress reaches the initial damage surface (**A**′), initiating crack growth this causes the damage surface to contract with further straining. Though the size of the damage surface starts to decrease immediately due to crack growth, the stress level in the material still increases with strain until a peak value (**B**) is reached. This is because the rate of damage accumulation, which is proportional to the square of the crack size, is small when the crack size is small, and the inelastic strain rate due to the crack growth ($\dot{\boldsymbol{\varepsilon}}_c^{gr}$ in Eq. (33b)) is too small to influence the total strain rate

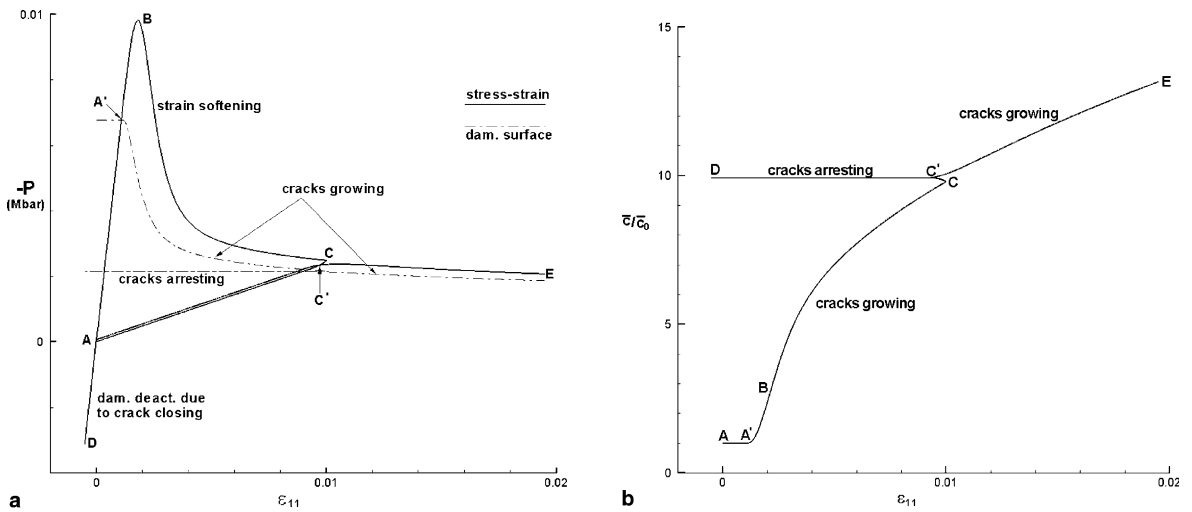

Fig. 6. The predicted response under hydrostatic (isotropic), cyclic loading: (a) pressure-strain response; (b) evolution of the crack size as a function of the strain.

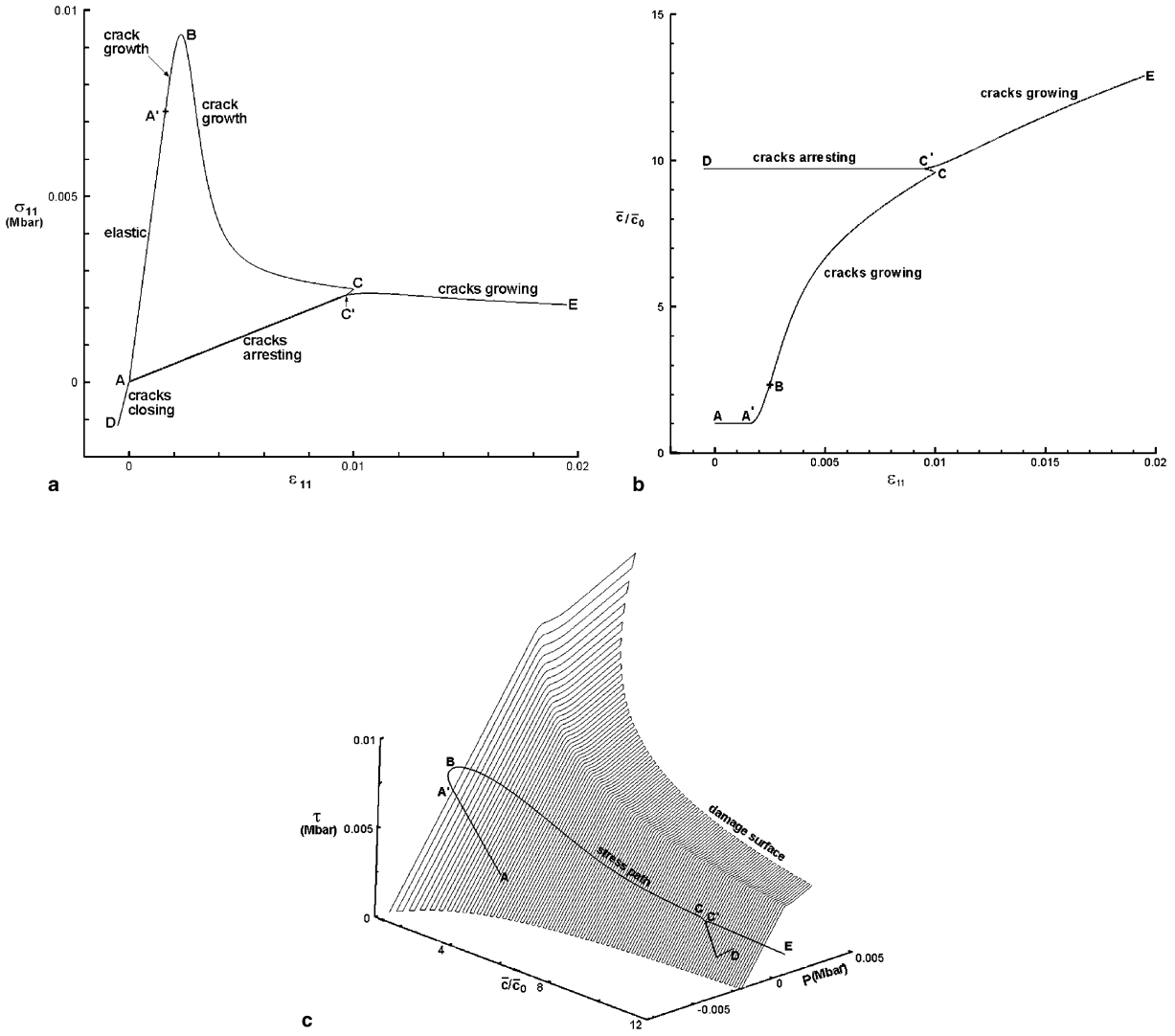

Fig. 7. The response of uniaxial strain, cyclic loading: (a) stress–strain response; (b) evolution of the crack size with strain; (c) stress path superimposed on the damage surface.

significantly. Consequently, the response remains "strain-hardening" (**A**′–**B**). Because $\dot{\varepsilon}_c^{gr}$ increases with crack size and distance from the stress state to the damage surface, for a given total strain rate $\dot{\boldsymbol{\varepsilon}}$, the inelastic strain rate $\dot{\boldsymbol{\varepsilon}}_c^{gr}$ eventually approaches the total strain rate and the material response changes from hardening to softening (**B**–**C**). This is in contrast to the rate-independent formulations, where the stress state is required to remain on the damage surface from the consistency condition, and softening would occur immediately after the stress state reaches the damage surface. In the current rate-dependent formulation, the stress state is allowed to be outside the damage surface by a distance proportional to the rate of loading.

The unloading path (**C**−**C**′−**A**) begins at **C** and, because the stress state is outside the damage surface, crack growth continues until the stress unloads enough to reach the surface (point **C**′). From **C**′, the material unloads elastically (with the damaged modulus) back to the origin (**A**), where both the matrix strain and

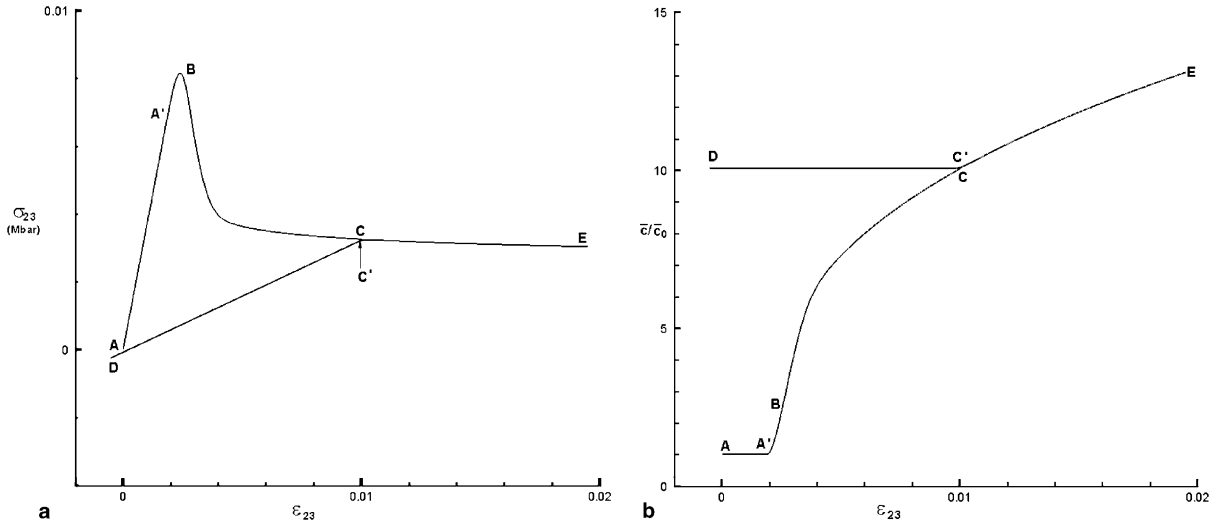

Fig. 8. The response of pure shear, cyclic loading: (a) stress–strain response; (b) evolution of the crack size with strain.

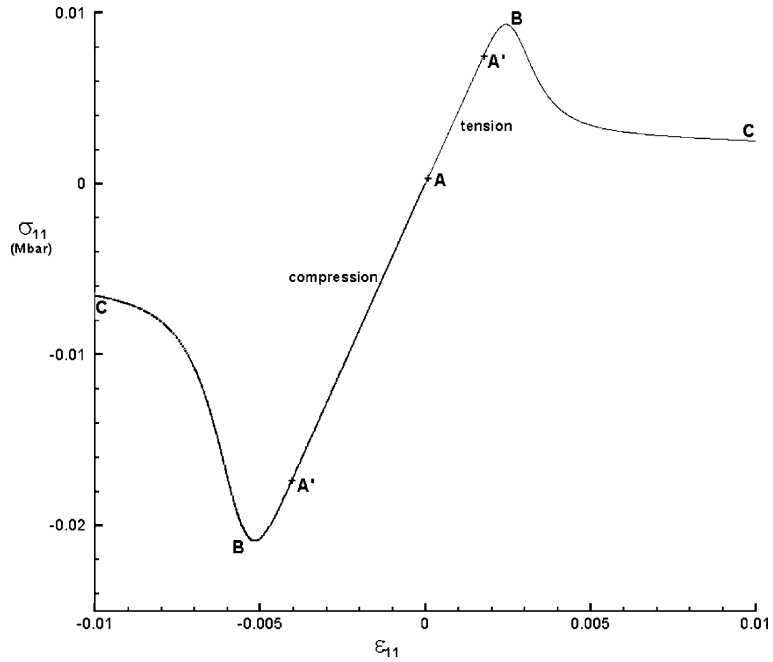

Fig. 9. Comparison of the behaviors under uniaxial stress for tensile and compressive loadings starting at **A**, the unstressed state.

crack strain are zero, and all the cracks are completely closed. The segment **A**−**D** corresponds to reverse loading (hydrostatic compression) of the damaged material with the crack size attained at **C**′ ($\bar{c}_1 \equiv \bar{c}' \approx 10\bar{c}_0$). Because the cracks remain closed under compression, damage accumulated in the material is deactivated (cracks of size $\bar{c}_1$ are still present). Consequently, the material assumes the original

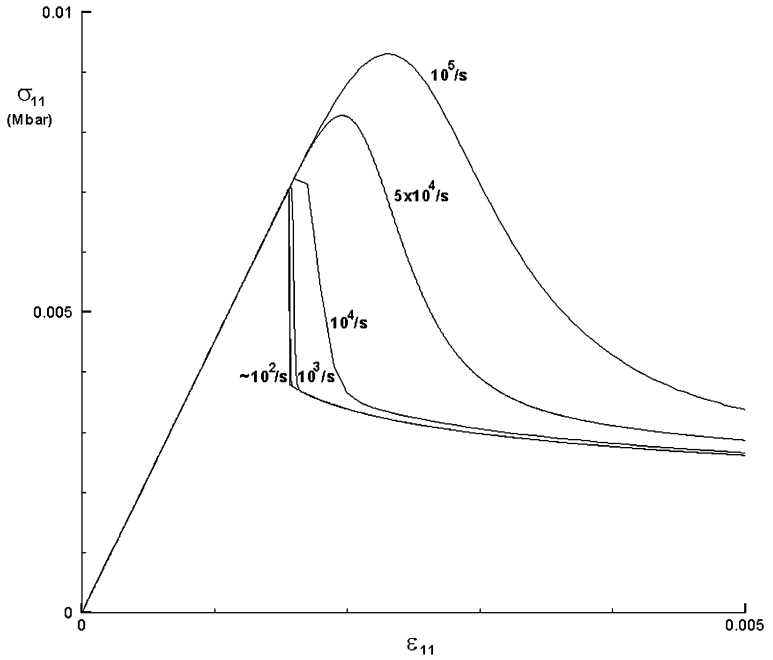

Fig. 10. The effects of loading rate on the material response.

(undamaged) stiffness. The reloading path (**D**−**A**−**C**′−**E**) starts from **D** and continues elastically with the undamaged stiffness back to the origin (**A**). On further loading, the cracks (with the increased size $\bar{c}_1$) open under tension and the damage, which has been accumulated at **C**′, becomes active again. Consequently, the reloading path follows the segment **A**−**C**′. The path intersects the damage surface at point **C**′, and the crack size again increases along the path **C**′−**E**. The stress state is outside the damage surface due to rate effects.

It is shown in Fig. 6b that the cracks are initially stable when the stress level is low (**A**−**A**′), become unstable at **A**′, and grow rapidly at first due to the high values of energy release rate, then slowly as the stress level drops. On unloading, the cracks continue to grow slightly (**C**−**C**′), and then arrest and remain stable (the stress state is inside the damage surface). During reloading, the cracks remain stable (**D**−**C**′) until the stress reaches the damage surface again at point **C**′. During the rest of the reloading path (**C**′−**E**), cracks continue to grow.

The uniaxial strain response, which is given in Fig. 7, shows features similar to the hydrostatic loading simulation discussed above. The strain rate and loading history are the same as for the hydrostatic loading. Since the material develops both pressure and shear stress under uniaxial strain loading, a three-dimensional plot showing the path of the stress state (p, τ) and crack size $(\bar{c})$ is provided in Fig. 7c. The damage surface is also superimposed on the stress path. Note that since the elastic portions of the stress path (i.e. **A**−**A**′ and **C**′−**D**) are inside the damage surface, they should be hidden by the surface but the computer graphics software does not have a hidden line removal capability. The uniaxial strain loading was also considered by Addessio and Johnson (1990) using ISOSCM. Predictions of the two models have similar features. For example, both models predict the initial linear elastic response with the slightly damaged modulus due to the small initial crack size until the stress state reaches the initial damage surface. Then there is a rapid decrease of stress (both tension and shear stress) as the result of fast crack growth. Both models show that the stress continues to decrease, but at a much slower rate, after the material has accumulated substantial damage (large crack size). The stress path evolves outside the damage surface when the

damage accumulates, as required by the rate-dependent formulation. The current model shows a much smoother response than the previous model.

The response for pure shear is shown in Fig. 8. The loading rate and history (loading-unloading-reloading) are the same as in the hydrostatic and uniaxial strain simulations. Features similar to the hydrostatic and uniaxial loading are observed. One main difference is that, upon reverse loading, the material does not recover the original, undamaged modulus. This is due to the fact that the maximum principal stress is always positive (tensile) under shear loading (reversing the shear direction only rotates the maximum principal direction by 90°). Consequently, the material damage is unchanged when the shear direction is reversed.

The responses for the conditions of tensile and compressive uniaxial-stress are compared in Fig. 9. Only the strain rate in the loading direction is specified ($\dot{\varepsilon}_{11} = \pm 10^5\ \mathrm{s}^{-1}$ for tension and compression, respectively). The strain rates in the lateral directions ($\dot{\varepsilon}_{22}, \dot{\varepsilon}_{33}$) are solved using the stress-free condition in those directions ($\sigma_{22} = \sigma_{33} = 0$). Both tension and compression responses show features similar to the other loading paths. That is, both load elastically until the initial damage surface is reached (**A′**), show first "strain-hardening" (increasing of stress with strain) before the peak stress (**B**) when crack size is small, and post-peak softening (**B-C**) when crack size is large enough. Because the positive projection operator ($\mathbf{P}^+$) for tension loading is different from that for compression loading ($\mathbf{P}^+ = \mathbf{0}$ for compression), the initial stiffness for tension is smaller than for compression. The stiffnesses appear to be the same in Fig. 9 because the initial damage is very small ($d_0 = N_0\bar{c}_0^3 = 0.27 \times 10^{-3}$) for the model material. We have increased the initial crack size from 14 μm to 140 μm, and the results (not shown) indeed show significant differences in the initial stiffnesses.

Fig. 9 also shows that the critical stresses for initial damage growth (**A′**) are significantly different for tensile and compressive loadings. The critical stress under uniaxial compression is more than twice that for uniaxial tension with a friction coefficient of only 0.26. This is a result of using the damage surface given in Section 2.3. Under uniaxial tension, the damage surface is given by Eq. (25), and the critical stress is $\sigma_t = \sigma_{11}^t = S_{\mathrm{cr}}(\bar{c}_0)/\sqrt{1-v/2}$. With the material constants for the SiC given in Table 1, the critical stress is $\sigma_t = 0.007$ Mbar. The damage surface for uniaxial compression is given by Eq. (26), and the compressive critical stress is $\sigma_c = -\sigma_{11}^c = 2(\sqrt{\mu^2+1}+\mu)S_{\mathrm{cr}}(\bar{c}_0)$. With $\mu = 0.26$, the compressive critical stress is $\sigma_c = 0.017$ Mbar. The numerical results shown in Fig. 9 reflect these theoretical predictions.

The ratio of compressive critical stress to tensile critical stress is $\sigma_c/\sigma_t = 2\sqrt{1-v/2}(\sqrt{\mu^2+1}+\mu)$, which increases with the friction coefficient μ . With $\mu = 0.26$, the ratio of compressive to tensile critical stresses for the SiC is 2.48. In clean microcracks where there may be significant cohesion the value of μ is much higher. For example, a friction coefficient of unity is used by McClintock and Walsh (1962) to study the effect of interfacial friction on the compressive strength of rocks. Their predicted compressive strength compares favorably with experimental data for a variety of rocks under different confining pressures. For $\mu = 1.0$ and Poisson's ratio $v = 0.2$, the current model gives the ratio of $\sigma_c/\sigma_t = 4.58$.

As discussed earlier, the current model is rate dependent (Eq. (31)). The rate effects on material response are shown in Fig. 10, where the results of six different loading rates (from $10\ \mathrm{s}^{-1}$ to $10^5\ \mathrm{s}^{-1}$) are given. It is seen that the stress increases first modestly with the strain rate for the rate up to$10^3\ \mathrm{s}^{-1}$, then dramatically for high strain rate ($> 10^3\ \mathrm{s}^{-1}$). This dramatic increase in the stress is due to the dynamic effects associated with the high speed crack growth (Freund, 1990).

5. Summary and conclusions

A rate-dependent, continuum damage model has been developed for the dynamic response of brittle materials containing an isotropic distribution of cracks. The current model (DCA, Dominant Crack Algorithm) is based on the ISOSCM model of Addessio and Johnson (1990) and recent work of Zuo and Dienes (2005) on the instability of penny-shaped cracks under general stress states. The main features

of the current model are the following: (1) A new damage surface, which defines the onset of damage evolution, is found by applying the generalized Griffith instability criterion for the critical (most unstable) crack orientation. The damage surface is a composite of four surfaces defining the stability of penny-shaped cracks. The four surfaces reflect the fact that the critical crack orientation strongly depends on the state of stress (e.g., the critical crack plane changes from being normal to the loading direction to being almost parallel to it when the loading changes from uniaxial tension to uniaxial compression). The new damage surface removes a discontinuity in the damage surface in ISOSCM, as the pressure in the material changes sign. (2) The crack strain due to crack opening is treated in a more physical manner in the current model. For the stress states where the principal stresses have mixed signs only the tensile principal stresses contribute to the crack opening strain. This is achieved by incorporating the positive projection operator in the equation for the crack opening strain. One important consequence is that classical dilatancy (volume increase due to shear), a physical feature of brittle materials, but not accounted for in ISOSCM, is included in the current model. (3) The evolution of damage, in terms of the growth rate of the mean crack size, is based on the energy-release rate for the dominant crack (having the critical orientation). The crack growth equation is based on the work of Freund (1990) on dynamic fracture. Since both the damage surface and growth are based on the same energy-release rate, the damage evolution equation has been cast into a form analogous to over-stress models for the rate-dependent plasticity formulations. In ISOSCM, the damage growth rate was assumed to be an exponential function of the distance of the stress state from the damage surface with no specific physical justification. The current formulation has a better physical basis than the ISOSCM formulation.

Both the explicit and an implicit algorithm for numerically integrating the evolution equations for stress and damage (mean crack size) have been developed for the model. A comparison of the numerical results using the two algorithms has been provided for uniaxial strain loading. The numerical results show that a larger time-step can be used with the implicit algorithm than with the explicit algorithm (ISOSCM uses the explicit algorithm). A driver program has been written which provides the strain history to the material subroutine for updating the material state (stress and mean crack size). Numerical simulations for a silicon carbide (SiC) ceramic under several loading paths (hydrostatic tension/compression, uniaxial strain, uniaxial stress, and shear) and different strain rates are presented to illustrate the main features of the model. The response to uniaxial strain loading predicted by the current model is similar to those using ISOSCM. The numerical results also show that the current model captures many important features of brittle materials under dynamic loading.

The linear volumetric response (EOS, Equation of the State) for the matrix material has been assumed in the current model for simplicity (although the response for the damaged material is still nonlinear when there is a tensile principal stress due to volumetric crack strain). This is appropriate for low-pressure applications, but when strong shock waves are generated, the nonlinear effects of the volumetric response cannot be neglected. Incorporating a nonlinear EOS and implementing the model into an analysis code are goals for future work. We also plan to apply the model to particular brittle materials (e.g., ceramics, propellants, explosives, and beryllium alloys) under high strain-rate loadings (e.g., plate impact and spall problems).

The current model also can be viewed as a simplified implementation of the SCRAM theory developed by Dienes, 1978, 1983a,b, 1996, a general approach to brittle behavior that accounts for opening, shear, growth and coalescence of cracks in the context of large deformations and extreme pressures and temperatures. Whereas Dienes' original implementation of SCRAM accounts for the individual development of cracks with different orientations (hence capturing anisotropic damage), the current implementation simplifies the algorithms and hence speeds up calculations by emphasizing the growth of cracks with the most unstable (critical) orientation. The number of material constants for the current model has been kept to a minimum. In addition to the elastic constants (mass density, shear modulus and Poisson's ratio), there are only 4 damage constants: the crack number density N_0 and initial crack size $\bar{c}_0$, which characterize the initial damage in the material; the effective surface energy γ and friction coefficient μ, which determine

crack growth (hence the evolution of damage). Having a small number of physically-based model constants can be advantageous in applications where an extensive set of material test data is not available.

The representation of brittle behavior with an ensemble of penny-shaped cracks has been used for many years at Los Alamos and elsewhere, but only recently have we formulated analytic criteria that define the orientation of the most unstable cracks and the critical condition, accounting for both open cracks and closed cracks with interfacial friction. This makes it possible to carry out calculations with precisely determined orientations for growth. This may prove to be significantly more efficient and effective than an alternative procedure that we have used that examines the individual stability of cracks with many different orientations. In a recent verification study of SCRAM, for example, the dynamic response of an axisymmetric thick ring to internal pressure was considered and we found that 30 orientations on the unit hemisphere are needed to get good accuracy and up to 480 orientations to get accuracy at the 2% level (Dienes et al., 2004). This situation arises because compression failure may occur within only a narrow range of orientations. The full machinery of SCRAM may be required in complex situations however, where numerous orientations become unstable at different times, a situation that can occur, for example, in impact on complex targets such as armor with multiple layers. Detailed studies are planned, but have not been initiated at this time.

The current model (DCA), like its predecessors (SCRAM, ISOSCM and Visco-SCRAM), is designed to account for the behavior of brittle materials, but in this implementation we are attempting to formulate the simplest viable model that accounts for the statistics of crack growth. Thus the effects of crack nucleation and coalescence (annihilation) during deformation, as well as interactions between cracks, are not accounted for, nor do we attempt to combine brittle and plastic behavior or nonlinearities in the equation of state. According to Kachanov (1993), for a solid with a given arrangement of cracks the effects of crack interactions on the effective elastic moduli of the solid may be very small. Crack coalescence can play an important role in the failure of brittle materials. However, at the early stage of damage when cracks are still too far apart to intersect each other, the effects of crack coalescence on damage are small (Dienes, 1996). Exclusion of crack nucleation in the model is partially justified by the fact that cracks of all sizes (from zero to infinite) are assumed to exist prior to loading. Crack coalescence, as well as crack hardening (R-curve behavior), crack inertia (onset and arrest), and hot spots in reactive materials are addressed in the full version of SCRAM (Dienes et al., 2005).

In summary, the procedure described herein appears to have the potential for significantly improved accuracy, but more precise calculations and experiments are needed to confirm the merits of this approach.

Acknowledgements

Los Alamos National Laboratory is operated by the University of California for the United States Department of Energy (DOE), under contract W-7405-ENG-36. This work was supported by the Joint DOE and Department of Defense (DoD) Munitions Technology Development Program, the DOE Advanced Simulation and Computing (ASC) Program, and by the US Army Research Laboratory. The authors are grateful for technical discussions with C.A. Bronkhorst, R.M. Hackett, P.J. Maudlin, and H.L. Schreyer.

Appendix A. The positive projection operator for a pure-shear stress state

To illustrate the procedure for finding the positive projection operator and activated open crack strain, consider a material under a pure-shear stress in some reference (e.g., Lab) basis given by $\mathbf{E}_\alpha$ ($\alpha = 1, 2, 3$). The stress is then

$$\boldsymbol{\sigma} = s(\mathbf{E}_2 \otimes \mathbf{E}_3 + \mathbf{E}_3 \otimes \mathbf{E}_2), \tag{A.1}$$

where $\mathbf{E}_2$–$\mathbf{E}_3$ defines the shear plane. Without loss of generality, it is assumed here that $s > 0$. The principal stresses and principal directions are

$$\sigma_1 = s, \quad \sigma_2 = 0, \quad \sigma_3 = -s, \tag{A.2a}$$

$$\mathbf{e}_1 = (\mathbf{E}_2 + \mathbf{E}_3)/\sqrt{2}, \quad \mathbf{e}_2 = \mathbf{E}_1, \quad \mathbf{e}_3 = (\mathbf{E}_2 - \mathbf{E}_3)/\sqrt{2}. \tag{A.2b}$$

The positive spectral tensor defined in Eq. (15a) is

$$\mathbf{Q}^+ = \mathbf{e}_1 \otimes \mathbf{e}_1 = \frac{1}{2}(\mathbf{E}_2 \otimes \mathbf{E}_2 + \mathbf{E}_3 \otimes \mathbf{E}_3 + \mathbf{E}_2 \otimes \mathbf{E}_3 + \mathbf{E}_3 \otimes \mathbf{E}_2). \tag{A.3a}$$

In the reference basis $(\mathbf{E}_\alpha)$, the components of Q^+ are

$$[\mathbf{Q}^+]_{\mathbf{E}_\alpha} = \frac{1}{2}\begin{bmatrix} 0 & 0 & 0 \\ 0 & 1 & 1 \\ 0 & 1 & 1 \end{bmatrix}. \tag{A.3b}$$

The positive projection operator and the projected stress are, using Eqs. (14) and (16a),

$$\mathbf{P}^+ = (\mathbf{e}_1 \otimes \mathbf{e}_1) \wedge (\mathbf{e}_1 \otimes \mathbf{e}_1) = \mathbf{e}_1 \otimes \mathbf{e}_1 \otimes \mathbf{e}_1 \otimes \mathbf{e}_1, \tag{A.4a}$$

$$\boldsymbol{\sigma}^+ \equiv \mathbf{P}^+\boldsymbol{\sigma} = (\mathbf{e}_1 \cdot \boldsymbol{\sigma} e_1)\mathbf{e}_1 \otimes \mathbf{e}_1 = \sigma_1 \mathbf{e}_1 \otimes \mathbf{e}_1 = s\mathbf{e}_1 \otimes \mathbf{e}_1. \tag{A.4b}$$

The components of $\boldsymbol{\sigma}^+$ are

$$[\boldsymbol{\sigma}^+]_{\mathbf{E}_\alpha} = \frac{s}{2}\begin{bmatrix} 0 & 0 & 0 \\ 0 & 1 & 1 \\ 0 & 1 & 1 \end{bmatrix}. \tag{A.5}$$

It can be readily verified that using the alternative formula $\boldsymbol{\sigma}^+ = \mathbf{Q}^+\boldsymbol{\sigma}\mathbf{Q}^+$, which involves only second-order tensors, yields identical results. The corresponding damage tensor $\mathbf{D}(\bar{c})$ given by Eq. (22) is

$$\mathbf{D}(\bar{c}) = \frac{3}{2}\beta^{\mathrm{e}} d(\bar{c})(\delta \mathbf{P}^{\mathrm{d}} + \mathbf{e}_1 \otimes \mathbf{e}_1 \otimes \mathbf{e}_1 \otimes \mathbf{e}_1), \tag{A.6}$$

where $d(\bar{c}) = N_0\bar{c}^3$ and $\delta \equiv 1/(1 - (\nu/2))$. In deriving the results, the following relations based on Eqs. (13b,c) have been used:

$$(\mathbf{e}_1 \otimes \mathbf{e}_1) : \mathbf{P}^{\mathrm{d}}(\mathbf{e}_1 \otimes \mathbf{e}_1) = \frac{2}{3}, \quad (\mathbf{e}_1 \otimes \mathbf{e}_1) : \mathbf{P}^{\mathrm{sp}}(\mathbf{e}_1 \otimes \mathbf{e}_1) = \frac{1}{3}. \tag{A.7}$$

The activated open-crack strain given by Eq. (13a) is

$$\boldsymbol{\varepsilon}_{\mathrm{c}}^{\mathrm{o}}(\boldsymbol{\sigma}, \bar{c}) = \beta^{\mathrm{e}} d(\bar{c})\left(\frac{3}{2}\mathbf{e}_1 \otimes \mathbf{e}_1 \otimes \mathbf{e}_1 \otimes \mathbf{e}_1\right)\boldsymbol{\sigma} = \beta^{\mathrm{e}} d(\bar{c})\left(\frac{3}{2}s\right)\mathbf{e}_1 \otimes \mathbf{e}_1. \tag{A.8}$$

Since $\mathrm{tr}\boldsymbol{\sigma} = 0$, the stress deviator is

$$\boldsymbol{\sigma}^{\mathrm{d}} = \boldsymbol{\sigma} = s(\mathbf{e}_1 \otimes \mathbf{e}_1 - \mathbf{e}_3 \otimes \mathbf{e}_3). \tag{A.9}$$

The total crack strain $\boldsymbol{\varepsilon}_{\mathrm{c}}(\boldsymbol{\sigma}, \bar{c})$ given by Eq. (17) is then

$$\boldsymbol{\varepsilon}_{\mathrm{c}}(\boldsymbol{\sigma}, \bar{c}) = \frac{3}{2}s\beta^{\mathrm{e}} d(\bar{c})(\delta(\mathbf{e}_1 \otimes \mathbf{e}_1 - \mathbf{e}_3 \otimes \mathbf{e}_3) + \mathbf{e}_1 \otimes \mathbf{e}_1), \tag{A.10a}$$

with the components in the Lab basis

$$[\boldsymbol{\varepsilon}_c]_{\mathbf{E}_\alpha} = \left(\frac{3}{2}\right) s\beta^e d(\bar{c}) \left(\delta \begin{bmatrix} 0 & 0 & 0 \\ 0 & 0 & 1 \\ 0 & 1 & 0 \end{bmatrix} + \frac{1}{2} \begin{bmatrix} 0 & 0 & 0 \\ 0 & 1 & 1 \\ 0 & 1 & 1 \end{bmatrix} \right). \tag{A.10b}$$

Laboratory tests indicate that when a brittle material is subject to a deviatoric stress (e.g., pure shear), its volume increases with stress, a phenomenon called dilatancy (e.g., Scholz, 2002). The stress state here is pure shear, so the volumetric crack strain is due to dilatancy. It follows from Eq. (A.10a) that the dilatancy is

$$\operatorname{tr}(\boldsymbol{\varepsilon}_c(\boldsymbol{\sigma}, \bar{c})) = \operatorname{tr}(\boldsymbol{\varepsilon}_c^o(\boldsymbol{\sigma}, \bar{c})) = \frac{3}{2} s\beta^e d(\bar{c}). \tag{A.10c}$$

In ISOSCM, Addessio and Johnson (1990) did not account for shear dilatancy, but suggested that it should be included in the future development. Dilatancy can result from crack opening under shear or from joint opening under shear. Here, we consider only the former mechanism. Joint or crack opening as a source of dilatancy has been incorporated in SCRAM and plays a role in the response of ceramic armor to impact (Meyer et al., 1999; Zuo et al., 2003).

In a computer algorithm for anisotropic material response it is more efficient and easier to manipulate and interpret numerical results if the stress and strain tensors are represented with six-dimensional vectors (Voigt–Mandel form). In the Voigt–Mandel form, the fourth-order compliance tensor is represented by a 6×6 matrix (e.g., Mason and Maudlin, 1999). The damage tensor $\mathbf{D}(\bar{c})$ given by Eq. (A.6) has a particularly simple matrix form in the principal basis of stress ($\mathbf{e}_1$–$\mathbf{e}_2$–$\mathbf{e}_3$):

$$[\mathbf{D}(\bar{c})]_{\mathrm{VM}} = \frac{3}{2}\beta^e d(\bar{c}) \left(\delta \begin{bmatrix} 2/3 & -1/3 & -1/3 & 0 & 0 & 0 \\ -1/3 & 2/3 & -1/3 & 0 & 0 & 0 \\ -1/3 & -1/3 & 2/3 & 0 & 0 & 0 \\ 0 & 0 & 0 & 1 & 0 & 0 \\ 0 & 0 & 0 & 0 & 1 & 0 \\ 0 & 0 & 0 & 0 & 0 & 1 \end{bmatrix} + \begin{bmatrix} 1 & 0 & 0 & 0 & 0 & 0 \\ 0 & 0 & 0 & 0 & 0 & 0 \\ 0 & 0 & 0 & 0 & 0 & 0 \\ 0 & 0 & 0 & 0 & 0 & 0 \\ 0 & 0 & 0 & 0 & 0 & 0 \\ 0 & 0 & 0 & 0 & 0 & 0 \end{bmatrix} \right). \tag{A.11}$$

In the principal basis, the Voigt–Mandel form of the stress is

$$\{\sigma\}_{\mathrm{VM}} = \{s, 0, -s, 0, 0, 0\}^{\mathrm{T}}, \tag{A.12}$$

where the superscript "T" denotes the transpose. The crack strain is then

$$\{\varepsilon_c\}_{\mathrm{VM}} = [\mathbf{D}(\bar{c})]_{\mathrm{VM}}\{\sigma\}_{\mathrm{VM}} = \frac{3}{2} s\beta^e d(\delta\{1, 0, -1, 0, 0, 0\}^{\mathrm{T}} + \{1, 0, 0, 0, 0, 0\}^{\mathrm{T}}), \tag{A.13}$$

which agrees with the tensor result given in Eq. (A.10a,b).

Appendix B. Damage moduli for the cases of isotropic damage

When the principal stresses are of the same sign (either all tensile or all compressive), the damage is isotropic in the current model. Since the matrix material is assumed to be isotropic, the damaged material remains isotropic, and the material response can be separated into deviatoric and spherical parts:

$$\boldsymbol{\varepsilon}^{\mathrm{d}} = \frac{\boldsymbol{\sigma}^{\mathrm{d}}}{2\widehat{G}(\bar{c})}, \quad \operatorname{tr}\boldsymbol{\varepsilon} = \frac{\operatorname{tr}\boldsymbol{\sigma}}{3\widehat{K}(\bar{c})}, \tag{B.1}$$

where $\boldsymbol{\varepsilon}^{\mathrm{d}} \equiv \boldsymbol{\varepsilon} - (\mathrm{tr}\,\boldsymbol{\varepsilon}/3)\mathbf{i}$ is the deviatoric part of strain tensor, and $\widehat{G}(\bar{c})$ and $\widehat{K}(\bar{c})$ are the shear and bulk moduli of the damaged material, respectively. Expressions for $\widehat{G}(\bar{c})$ and $\widehat{K}(\bar{c})$ for the cases where the stress state is either pure-compression (B.1) or pure-tension (B.2) are derived below.

B.1. Material is in pure-compression ($0 \geqslant \sigma_1 \geqslant \sigma_2 \geqslant \sigma_3$)

Since the principal stresses are compressive, all cracks are closed. It follows from the definitions (Eqs. (14a)–(15a)) that $\mathbf{Q}^{+} = \mathbf{o}$ and $\mathbf{P}^{+} = \mathbf{O}$, null tensors. The damage tensor given by Eq. (22) is purely deviatoric:

$$\mathbf{D}(\bar{c}) = \frac{3}{2-\nu}\beta^{\mathrm{e}} N_0 \bar{c}^3 \mathbf{P}^{\mathrm{d}}. \tag{B.2}$$

Multiplying the stress–strain relation (Eq. (20)) by the deviatoric projection operator ($\mathbf{P}^{\mathrm{d}}$) gives

$$\boldsymbol{\varepsilon}^{\mathrm{d}}(\boldsymbol{\sigma}, \bar{c}) = \left(\frac{1}{2G} + \frac{3\beta^{\mathrm{e}}}{2-\nu} N_0 \bar{c}^3\right)\boldsymbol{\sigma}^{\mathrm{d}}. \tag{B.3}$$

The damage shear modulus is found by comparing Eqs. (B.3) and (B.1):

$$\widehat{G}(\bar{c}) = \frac{G}{1 + \gamma_c^{\mathrm{e}} N_0 \bar{c}^3}, \quad \gamma_c^{\mathrm{e}} \equiv \frac{128\pi}{5}\frac{1-\nu}{2-\nu}. \tag{B.4}$$

The elastic constant γ_c^{e} changes only slightly with the Poisson's ratio.

Since the damage tensor is purely deviatoric, there is no influence of damage in the bulk modulus, and the volumetric response is linear elastic with the matrix's bulk modulus, $\widehat{K}(\bar{c}) = K$.

B.2. Material is in pure-tension ($\sigma_1 \geqslant \sigma_2 \geqslant \sigma_3 > 0$)

It follows from Eqs. (14a) and (15a) that $\mathbf{Q}^{+} = \mathbf{i}$ and $\mathbf{P}^{+} = \mathbf{I}$. The damage tensor given by Eq. (22) has both deviatoric and spherical parts,

$$\mathbf{D}(\bar{c}) = \beta^{\mathrm{e}} N_0 \bar{c}^3 \left(\frac{5-\nu}{2-\nu}\mathbf{P}^{\mathrm{d}} + \frac{5}{2}\mathbf{P}^{\mathrm{sp}}\right). \tag{B.5}$$

The deviatoric response and spherical response are found by multiplying Eq. (20) by the deviatoric projection operator ($\mathbf{P}^{\mathrm{d}}$) and the spherical projection operator ($\mathbf{P}^{\mathrm{sp}}$), respectively,

$$\boldsymbol{\varepsilon}^{\mathrm{d}}(\boldsymbol{\sigma}, \bar{c}) = \left(\frac{1}{2G} + \frac{5-\nu}{2-\nu}\beta^{\mathrm{e}} N_0 \bar{c}^3\right)\boldsymbol{\sigma}^{\mathrm{d}}, \tag{B.6a}$$

$$\mathrm{tr}\,\boldsymbol{\varepsilon} = \left(\frac{1}{3K} + \frac{5}{2}\beta^{\mathrm{e}} N_0 \bar{c}^3\right)\mathrm{tr}\,\boldsymbol{\sigma}. \tag{B.6b}$$

Comparing Eq. (B6) with Eq. (B.1) gives

$$\frac{1}{2\widehat{G}(\bar{c})} = \frac{1}{2G} + \frac{5-\nu}{2-\nu}\beta^{\mathrm{e}} N_0 \bar{c}^3,$$

$$\frac{1}{3\widehat{K}(\bar{c})} = \frac{1}{3K} + \frac{5}{2}\beta^{\mathrm{e}} N_0 \bar{c}^3.$$

Thus, the damage moduli are

$$\widehat{G}(\bar{c}) = \frac{G}{1 + \gamma_t^{\mathrm{e}} N_0 \bar{c}^3}, \quad \gamma_t^{\mathrm{e}} \equiv \frac{128\pi}{15} \frac{(5-\nu)(1-\nu)}{2-\nu}, \tag{B.7a, b}$$

$$\widehat{K}(\bar{c}) = \frac{K}{1 + \kappa^{\mathrm{e}} N_0 \bar{c}^3}, \quad \kappa^{\mathrm{e}} \equiv \frac{64\pi}{3} \frac{1-\nu^2}{1-2\nu}. \tag{B.8a, b}$$

For a typical value of $\nu = 0.25$, the elastic constants relating the reduction in shear and bulk moduli to the scalar damage measure ($d(\bar{c}) = N_0 \bar{c}^3$) are $\gamma_c^{\mathrm{e}} = 34.5$, $\gamma_t^{\mathrm{e}} = 54.6$ and $\kappa^{e} = 125.7$. It follows from Eqs. (B4) and (B7b) that $\gamma_t^{\mathrm{e}} = ((5-\nu)/3)\gamma_c^{\mathrm{e}} > \gamma_c^{\mathrm{e}}$. Thus, for the same amount of damage $d(\bar{c})$, the reduction in the shear modulus is greater when the material is under tensile loading than under compressive loading. This is because a tensile loading causes cracks to open and hence creates crack opening strain which has both spherical and deviatoric components (Eq. (5a)); the deviatoric component induces an additional reduction in the shear modulus.

Addessio and Johnson (1990) suggested that $d(\bar{c}) = 2.0$ approximately corresponds to the complete loss of load-carrying capacity (hence failure) of a brittle material. It has also been suggested (e.g, Rajendran, 1994) that a critical value of crack density can be used to predict failure of brittle materials. For $d(\bar{c}) = 2.0$, the damaged shear and bulk moduli are degraded to a small percentage of their undamaged values (1.4%, 0.9% and 0.4%, for compressive shear, tensile shear, and tensile bulk moduli, respectively).

When the principal stresses are of mixed signs (e.g., when the material is subjected to pure shear), the damage tensor is no long isotropic, consequently, the material response cannot be fully described by the shear and bulk moduli alone.

References

Addessio, F.L., Johnson, J.N., 1990. A constitutive model for the dynamic response of brittle materials. Journal of Applied Physics 67, 3275–3286.

Addessio, F.L., Johnson, J.N., 1993. Rate-dependent ductile failure model. Journal of Applied Physics 73, 1640–1648.

Alpa, G., 1984. On a statistical approach to brittle rupture for multiaxial states of stress. Engineering Fracture Mechanics 19, 881–901.

Batchelor, G.K., 1967. An Introduction to Fluid Dynamics. Cambridge University Press, Cambridge.

Bennett, J.G., Haberman, K.S., Johnson, J.N., Asay, B.W., Henson, B.F., 1998. A constitutive model for the non-shock ignition and mechanical response of high explosives. Journal of the Mechanics and Physics of Solids 46, 2303–2322.

Budiansky, B., O'Connell, R.J., 1976. Elastic moduli of a cracked solid. International Journal of Solids and Structures 12, 81–97.

Costin, L.S., 1983. A microcrack damage model for the deformation and failure of brittle rock. Journal of Geophysics Research 88, 9485–9492.

Curran, D.R., Seaman, L., Shockey, D.A., 1987. Dynamic failure of solids. Physics Report 147, 253–288.

Curran, D.R., Seaman, L., 1996. Simplified models of fracture and fragmentation. In: Davison, L., Grady, D.E., Shahinpoor, M. (Eds.), High Pressure Shock Compression of Solids II. Springer Verlag, New York, pp. 340–365.

Dienes, J.K., 1978. A statistical theory of fragmentation. In: Kim, Y.S. (Ed.), Proceedings of the 19th US Symposium on Rock Mechanics. University of Nevada, pp. 51–55.

Dienes, J.K., Margolin, L.G., 1980. A Computational approach to rock fragmentation. In: Summers, D.A. (Ed.), The state of the art in rock mechanics—Proceedings of Symposium on Rock Mechanics, pp. 390–399.

Dienes, J.K., 1981. On the effect of anisotropy in explosive fragmentation. In: Einstein, H.H. (Ed.), Rock Mechanics from Research to Application—Proceedings of the 22nd US Symposium on Rock Mechanics. M.I.T., Cambridge, MA.

Dienes, J.K., 1982. A frictional hot-spot theory for propellant sensitivity. In: Proceedings of 2nd JANNAF Propulsion Systems Hazards Subcommittee Meeting, Naval Weapons Center, China Lake, CA, pp. 269–278.

Dienes, J.K., 1983a. Statistical crack mechanics. In: Boehler, J.P. (Ed.), Proceedings of the Colloque Internationale du CNRS no. 351: Failure criteria of structured media, Villard-de-Lans, France, pp. 399–407.

Dienes, J.K., 1983b. On the stability of shear cracks and the calculation of compressive strength. Journal of Geophysics Research 88, 1173–1179.

Dienes, J.K., 1985. A statistical theory of fragmentation processes. Mechanics of Materials 4, 325–335.

Dienes, J.K., 1989. Theory of deformation, part II, physical theory. Los Alamos National Laboratory Report LA-11063-MS, Vol. II.
Dienes, J.K., 1996. A unified theory of flow, hot spots, and fragmentation with an application to explosive sensitivity. In: Davison, L., Grady, D.E., Shahinpoor, M. (Eds.), High Pressure Shock Compression of Solids II. Springer Verlag, New York, pp. 366–398.
Dienes, J.K., Middleditch, J., Zuo, Q.H., Kershner, J.D., 2004. On the role of crack orientation in brittle failure. In: Furnish, M.D., Gupta, Y.M., Forbers, J.W. (Eds.), Shock Compression of Condensed Matter—2003, AIP Conference Proceedings, 706. Springer-Verlag, New York, pp. 447–450.
Dienes, J.K., Zuo, Q.H., Kershner, J.D., 2005. Impact initiation of explosives and propellants via statistical crack mechanics. Journal of Physics and Mechanics of Solids, under review. LA-14226-MS, Los Alamos National Laboratory Report.
Dube, J.F., Pijaudier-Cabot, G., La Borderie, C., 1996. Rate dependent damage model for concrete in dynamics. Journal of Engineering Mechanics 122, 939–947.
Freund, L.B., 1972. Crack propagation in an elastic solid subjected to general loading –I. constant rate of extension. Journal of Mechanics and Physics of Solids 20, 129–140.
Freund, L.B., 1990. Dynamic Fracture Mechanics. Cambridge University Press, New York.
Gambarotta, L., Lagomarsino, S., 1993. A microcrack damage model for brittle materials. International Journal of Solids and Structures 30, 177–198.
Grady, D.E., 1989. Shock-wave strength properties of baron carbide and silicon carbide. Journal de Physique 4, 385–391.
Grady, D.E., Kipp, M.E., 1985. Geometric statistics and dynamic fragmentation. Journal of Applied Physics 58, 1210–1222.
Gurtin, M.E., 1981. An Introduction to Continuum Mechanics. Academic Press, New York.
Hackett, R.M., Bennett, J.G., 2000. An implicit finite element material model for energetic particulate composite materials. International Journal for Numerical Methods in Engineering 49, 1191–1209.
Hansen, N.R., Schreyer, H.L., 1994. A thermodynamically consistent framework for theories of elastoplasticity coupled with damage. International Journal of Solids and Structures 31, 359–389.
Hansen, N.R., Schreyer, H.L., 1995. Damage deactivation. Journal of Applied Mechanics 62, 450–458.
Kachanov, M., 1993. Elastic solids with many cracks and related problems. Advances in Applied Mechanics 30, 259–445.
Kanninen, M.F., Popelar, C.H., 1985. Advanced Fracture Mechanics. Oxford University Press, New York.
Keer, L.M., 1966. A note on shear and combined loading for a penny-shaped crack. Journal of Mechanics and Physics of Solids 14, 1–6.
Kipp, M.E., Grady, D.E., 1989a. Shock compression and release in high-strength ceramics. In: Schmidt, S.C., Johnson, J.N., Davison, L.W. (Eds.), Shock Compression of Condensed Matter, Proceedings of the American Physical Society Topical Conference, August 14–17, 1989, Albuquerque, New Mexico, pp. 377–380.
Kipp, M.E., Grady, D.E., 1989b. Shock compression and release in high-strength ceramics. Sandia National Laboratories Technical Report SAND89-1461.
Krajcinovic, D., 1984. Continuum Damage Mechanics. Applied Mechanics Review 37, 1–6.
Krajcinovic, D., 1989. Damage Mechanics. Mechanics of Materials 8, 117–197.
Krajcinovic, D., 1996. Damage Mechanics. North-Holland, Elsevier, Amsterdam, The Netherlands.
Krajcinovic, D., 1998. Selection of damage parameter- art or science?. Mechanics of Materials 28, 165–179.
Lee, H.K., Simunovic, S., Shin, D.K., 2004. A computational approach for prediction of the damage evolution and crushing behavior of chopped random fiber composites. Computational Materials Science 29, 459–474.
Lemaitre, J., Chaboche, J.-L., 1990. Mechanics of Solid Materials, English Translation. Cambridge University Press, New York.
Lewis, M.W., 1991. Investigation of a thermodynamically consistent, dynamic brittle damage constitutive model for ceramics. Masters Thesis, Department of Mechanical Engineering, The University of New Mexico, Albuquerque, NM.
Lewis, M.W., Schreyer, H.L., 1996. A thermodynamically consistent description of dynamic continuum damage. In: Davison, L., Grady, D.E., Shahinpoor, M. (Eds.), High Pressure Shock Compression of Solids II. Springer Verlag, New York, pp. 452–471.
Lubliner, J., 1990. Plasticity Theory. Macmillan Publishing Company, New York.
Mason, T.A., Maudlin, P.J., 1999. Effects of higher-order anisotropic elasticity using textured polycrystals in three-dimensional wave propagation problems. Mechanics of Materials 31, 861–882.
McClintock, F.A., Walsh, J.B., 1962. Friction on Griffith cracks in rocks under pressure. In: Rosenberg, R.M. (Ed.), Proceedings of the Fourth US National Congress of Applied Mechanics. ASME, New York, pp. 1015–1021.
Meyers, M.A., 1994. Dynamic Behavior of Materials. John Wiley & Sons, Inc., New York.
Meyer Jr., H.W., Abeln, T., Bingert, S., Bruchey, W.J., Brannon, R.M., Chhabildas, L.C., Dienes, J.K., Middleditch, J., 1999. Crack behavior of ballistically impacted ceramic. In: Furnish, M.D., Chhabildas, L.C., Hixson, R.S. (Eds.), Shock Compression of Condensed Matter, AIP Conference Proceedings, 505. Springer-Verlag, New York, pp. 1109–1112.
Nemat-Nasser, S., Hori, M., 1999. Micromechanics: Overall Properties of Heterogeneous Materials, second revised ed. North-Holland, Elsevier, Amsterdam, The Netherlands.
Oda, M., 1983. A method for evaluating the effect of crack geometry on the mechanical behavior of cracked rock masses. Mechanics of Materials 2, 163–171.

Oda, M., Suzuki, K., Maeshibu, T., 1984. Elastic compliance for rock-like materials with random cracks. Soils and Foundations 24, 27–40.

Rajendran, A.M., Kroupa, J.L., 1989. Impact damage model for ceramic materials. Journal of Applied Physics 66, 3560–3565.

Rajendran, A.M., 1994. Modeling the impact behavior of AD85 ceramic under multiaxial loading. International Journal of Impact Engineering 15, 749–768.

Rajendran, A.M., Grove, D.J., 1996. Modeling the shock response of silicon carbide, baron carbide and titanium diboride. International Journal of Impact Engineering 18, 611–631.

Rice, J.R., 1984. Comments on 'On the stability of shear cracks and the calculation of compressive strength' by J.K. Dienes. Journal of Geophysics Research 89, 2505–2507.

Sack, R.A., 1946. Extension of Griffith's theory of rupture to three dimensions. Proceedings of Physics Society 58, 729–736.

Scholz, C.H., 2002. The Mechanics of Earthquakes and Faulting, second ed. Cambridge University Press, New York.

Segedin, C.M., 1950. Note on a penny-shaped crack under shear. Proceedings of the Cambridge Philosophical Society 47, 396–400.

Seaman, L., Curran, D.R., Shockey, D.A., 1976. Computational models for ductile and brittle fracture. Journal of Applied Physics 47, 4811–4826.

Seaman, L., Curran, D.R., Murri, W.J., 1985. A continuum model for dynamic tensile microfracture and fragmentation. Journal of Applied Mechanics 52, 593–600.

Simo, J.C., Ju, J.W., 1987. Stress and strain based continuum damage models, parts I and II. International Journal of Solids and Structures 23, 821–869.

Simo, J.C., Ju, J.W., 1989. On continuum damage-elastoplasticity at finite strains: a computational framework. Computational Mechanics 5, 375–400.

Taylor, L.M., Chen, E.P., Kuszmaul, J.S., 1986. Microcrack-induced damage accumulation in brittle rock under dynamic loading. Computer Methods in Applied Mechanics and Engineering 55, 301–320.

Zhang, Y.Q., Hao, H., Lu, Y., 2003. Anisotropic dynamic damage and fragmentation of rock materials under explosive loading. International Journal of Engineering Science 41, 917–929.

Zuo, Q.H., Dienes, J.K., 2002. On the types of brittle failure. LA-13962-MS, Los Alamos National Laboratory Report.

Zuo, Q.H., Dienes, J.K., 2005. On the stability of penny-shaped cracks with friction: the five types of brittle behavior. International Journal of Solids and Structures 42, 1309–1326.

Zuo, Q.H., Dienes, J.K., Middleditch, J., Meyer, H.W., 2003. Modeling the damage in ceramic armor via statistical crack mechanics. In: Proceedings (CD-ROM) of the 2003 SEM Annual Conference and Exposition on Experimental and Applied Mechanics, Charlotte, NC, June 2–4, 2003, Society for Experimental Mechanics, Inc., Bethel, CT, Paper Number 246, 9 pp.